

Selective activation of G α ob by an adenosine A₁ receptor agonist elicits analgesia without cardiorespiratory depression

Mark J. Wall ^{1,10}✉, Emily Hill ^{1,10}, Robert Huckstepp ^{1,10}, Kerry Barkan^{2,10}, Giuseppe Deganutti ^{3,4,10}, Michele Leuenberger ^{5,10}, Barbara Preti^{5,10}, Ian Winfield^{2,10}, Sabrina Carvalho², Anna Suchankova², Haifeng Wei⁶, Dewi Safitri ^{2,7}, Xianglin Huang², Wendy Imlach ⁸, Circe La Mache ¹, Eve Dean¹, Cherise Hume¹, Stephanie Hayward¹, Jess Oliver¹, Fei-Yue Zhao⁶, David Spanswick ^{6,8,9}, Christopher A. Reynolds ^{3,4}, Martin Lochner ⁵, Graham Ladds ²✉ & Bruno G. Frenguelli ¹✉

The development of therapeutic agonists for G protein-coupled receptors (GPCRs) is hampered by the propensity of GPCRs to couple to multiple intracellular signalling pathways. This promiscuous coupling leads to numerous downstream cellular effects, some of which are therapeutically undesirable. This is especially the case for adenosine A₁ receptors (A₁R) whose clinical potential is undermined by the sedation and cardiorespiratory depression caused by conventional agonists. We have discovered that the A₁R-selective agonist, benzyloxy-cyclopentyladenosine (BnOCPA), is a potent and powerful analgesic but does not cause sedation, bradycardia, hypotension or respiratory depression. This unprecedented discrimination between native A₁R arises from BnOCPA's unique and exquisitely selective activation of G α ob among the six G α i/o subtypes, and in the absence of β -arrestin recruitment. BnOCPA thus demonstrates a highly-specific G α -selective activation of the native A₁R, sheds new light on GPCR signalling, and reveals new possibilities for the development of novel therapeutics based on the far-reaching concept of selective G α agonism.

¹School of Life Sciences, University of Warwick, Gibbet Hill Rd, Coventry CV4 7AL, UK. ²Department of Pharmacology, University of Cambridge, Tennis Court Road, Cambridge CB2 1PD, UK. ³Centre for Sport, Exercise and Life Sciences (CELS), Faculty of Health and Life Sciences, Coventry University, Coventry CV1 2DS, UK. ⁴School of Biological Sciences, University of Essex, Wivenhoe Park, Colchester CO4 3SQ, UK. ⁵Institute of Biochemistry and Molecular Medicine, University of Bern, 3012 Bern, Switzerland. ⁶NeuroSolutions Ltd, Coventry, UK. ⁷Pharmacology and Clinical Pharmacy Research Group, School of Pharmacy, Bandung Institute of Technology, Bandung 40132, Indonesia. ⁸Department of Physiology, Monash Biomedicine Discovery Institute, Monash University, Innovation Walk, Clayton, VIC 3800, Australia. ⁹Warwick Medical School, University of Warwick, Gibbet Hill Rd, Coventry CV4 7AL, UK. ¹⁰These authors contributed equally: Mark J. Wall, Emily Hill, Robert Huckstepp, Kerry Barkan, Giuseppe Deganutti, Michele Leuenberger, Barbara Preti, Ian Winfield. ✉email: mark.wall@warwick.ac.uk; grl30@cam.ac.uk; b.g.frenguelli@warwick.ac.uk

G protein-coupled receptors (GPCRs) are the targets of many FDA-approved drugs^{1,2}. However, the promiscuity with which they couple to multiple G protein- and β -arrestin-activated intracellular signalling cascades leads to unwanted side effects. These side effects limit both the range of GPCRs suitable for drug-targeting, and the number of conditions for which treatments could be developed^{3,4}. One family of GPCRs that have particularly suffered as drug targets from their promiscuous coupling and wide-ranging cellular actions are the four GPCRs for the purine nucleoside adenosine, despite the potential for using adenosine receptor agonists to treat many pathological conditions including cancer, and various cardiovascular, neurological and inflammatory diseases^{5–7}. For example, activation of the widely-distributed adenosine A₁ receptor (A₁R) with currently available agonists elicits multiple actions in both the central nervous system (CNS) and the cardiorespiratory system. In the CNS A₁Rs inhibit synaptic transmission, induce neuronal hyperpolarization, reduce seizure activity and cause sedation, while in the cardiorespiratory system A₁Rs slow the heart (bradycardia), and contribute to reducing blood pressure (hypotension), and depress respiration (dyspnoea)^{7–12}. These multiple effects severely limit the prospects of A₁R agonists as life-changing medicines, despite their potential use in a wide range of clinical conditions, such as glaucoma, type 2 diabetes mellitus, pain, epilepsy and cerebral ischaemia^{7,13–16}, and in which there are clear unmet clinical needs that could be addressed with novel therapeutics.

The therapeutic limitations of promiscuous GPCR coupling might be overcome through the development of biased agonists—compounds that preferentially recruit one intracellular signalling cascade over another^{4,17,18}. This signalling bias has most frequently been expressed in terms of G α vs β -arrestin signalling¹⁹ and has been pursued at a variety of receptors^{20,21}, for example, at the angiotensin II type 1 receptor (AT1R)²², and at neurotensin receptors in the treatment of drug addiction²³. Agonist bias has been sought in the context of opioid receptors, but with some controversy²⁴, for compounds producing analgesia with reduced respiratory depression, gastrointestinal disturbance and tolerance⁴.

However, while other forms of bias exist, including between individual G α subunits^{17,25,26}, the challenge remains in translating GPCR signalling bias observed *in vitro* to tangible, and physiologically- and clinically-relevant, selectivity at native receptors *in vivo*^{3,4,27,28}. Accordingly, while the potential to preferentially drive the G protein-coupling of A₁Rs has been described in several *in vitro* studies^{29–32}, to date no A₁R-specific agonist has been reported that can elicit biased G α agonism at native A₁Rs in intact physiological systems, let alone the selective activation of one G α subunit. To achieve such selectivity among G α subunits would introduce novel therapeutic opportunities across a wide range of debilitating clinical conditions.

Here we show, utilising molecular dynamics (MD) simulations, and G α i/o subunit- and β -arrestin-specific cellular signalling assays, how one A₁R-selective agonist, BnOCPA^{33,34}, fulfils the criteria for a selective G α agonist in exclusively activating G α ob among the six members of the G α i/o family of G protein subunits, and in the absence of β -arrestin recruitment. In addition, through a combination of CNS electrophysiology, physiological recordings of cardiorespiratory parameters, a sensitive assay of attention and locomotor function, and the use of a clinically-relevant model of chronic neuropathic pain, we demonstrate selective activation of native A₁Rs and the delivery of potent analgesia without sedation, motor impairment or cardiorespiratory depression. Our data thus demonstrate the translation of agonist G α selectivity *in vitro* to therapeutically tangible clinically-relevant observations *in vivo*. Such observations reveal the possibility of achieving G α selectivity

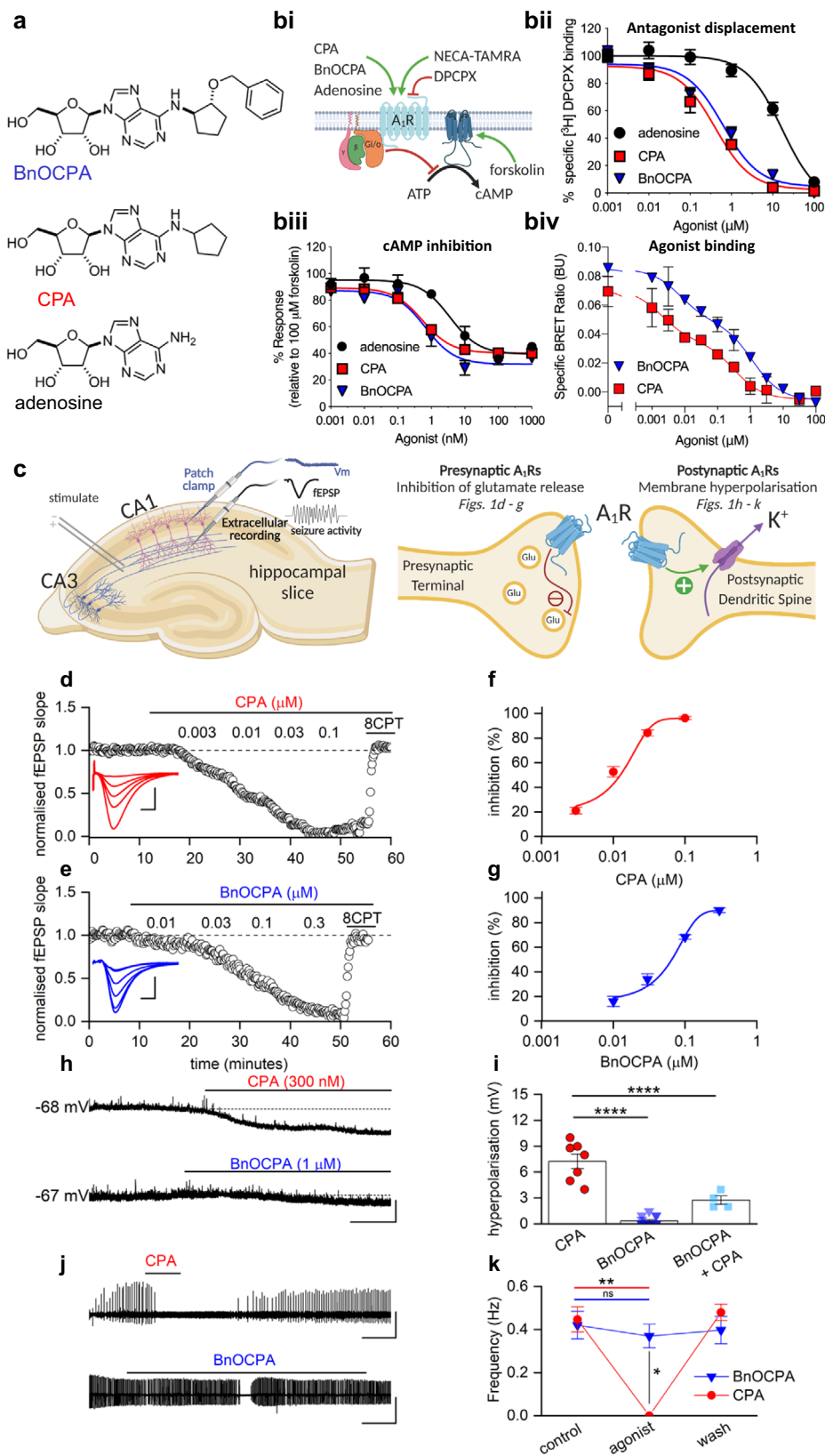
at native receptors, highlight the physiological benefits of such selectivity, and specifically speak to the possibility of unlocking the widespread clinical potential of A₁R agonists.

Results

The novel A₁R agonist BnOCPA exquisitely discriminates between native pre- and postsynaptic A₁Rs in the intact mammalian CNS. BnOCPA (Fig. 1a), a molecule first described in a patent as a potential treatment for glaucoma or ocular hypertension³⁴, is a cyclopentyl derivative of adenosine and a highly selective and potent, full agonist at human adenosine A₁Rs (hA₁Rs; Fig. 1b; Supplementary Table 1)³³. Our characterisation of BnOCPA, synthesised independently as part of a screen for suitable scaffolds for the generation of fluorescent ligands for the A₁R, began with an exploration of the binding characteristics of BnOCPA at the hA₁R using classical radioligand binding (where the antagonist [³H]DPCPX was used as a tracer), and a NanoBRET agonist binding assay (using a novel NECA-TAMRA compound, which acts as a full agonist (pEC₅₀ -7.23 ± 0.13 ; See Methods). Using both assays we observed that BnOCPA was able to bind to the hA₁R with an affinity equal to that of the prototypical A₁R agonists CPA and NECA, and higher than that of the endogenous agonist adenosine (Fig. 1b; Supplementary Table 1). Significantly, using NECA-TAMRA as the fluorescent agonist tracer, the high-affinity state of the biphasic binding profile observed in the NanoBRET assay was equivalent to that reported previously for BnOCPA (3.8 nM compared to 1.7 nM³⁴).

These initial pharmacological studies at recombinant hA₁Rs in cell lines did not reveal anything extraordinary about BnOCPA. However, when we investigated BnOCPA at native A₁Rs in rat hippocampal slices, against which BnOCPA is also a potent agonist, with ~8000- and >150-fold greater efficacy at rat A₁Rs (rA₁Rs) than at rat A_{2A}Rs (rA_{2A}Rs) and A₃Rs (rA₃Rs), respectively (Supplementary Table 2), we discovered properties of BnOCPA that were not consistent with those of typical A₁R agonists such as adenosine, CPA and NECA. In accordance with the effects of standard A₁R agonists, BnOCPA potently inhibited excitatory synaptic transmission in rat hippocampal slices (IC₅₀ ~65 nM; Fig. 1c–g and Supplementary Fig. 1a–d). This effect was attributable to the activation of native presynaptic A₁Rs on glutamatergic terminals⁹ (Fig. 1c; Supplementary Fig. 1e, f), and cannot be attributed to any action of BnOCPA at A₃Rs since even a high concentration (1 μ M) of the potent and selective A₃R agonist 2-Cl-IB-MECA³⁵ had no effect on synaptic transmission (Supplementary Fig. 1g, h). However, in stark contrast to adenosine and CPA, BnOCPA did not activate postsynaptic A₁Rs (Fig. 1c) to induce membrane hyperpolarisation, even at concentrations 15 times the IC₅₀ for the inhibition of synaptic transmission (Fig. 1h, i).

This peculiar and unique discrimination between pre- and postsynaptic A₁Rs might possibly be explained in terms of either some hindrance in the binding of BnOCPA to A₁Rs on postsynaptic neurones, or, and unprecedented for an A₁R agonist, binding to the postsynaptic A₁R, but without the ability to activate the receptor. To test the latter hypothesis—that BnOCPA actually bound to postsynaptic A₁Rs, but without efficacy—we reasoned that BnOCPA might behave in a manner analogous to a receptor antagonist in preventing or reversing activation by other A₁R agonists, a property that has been predicted and observed for biased agonists at other receptors^{17,27}. To test this, we pre-applied BnOCPA and then applied CPA (in the continued presence of BnOCPA). Remarkably, the co-application of CPA and BnOCPA resulted in a significant reduction of the effects of CPA on membrane potential (Fig. 1i; Supplementary Fig. 2a, b). In addition, membrane hyperpolarisation induced by the endogenous



agonist adenosine was reversed by BnOCPA (Supplementary Fig. 2c). In contrast, the A₃R agonist 2-Cl-IB-MECA had no effect on membrane potential and did not interfere with the membrane hyperpolarisation caused by adenosine (Supplementary Fig. 2d, e), further reaffirming the actions of BnOCPA as being selectively mediated by A₁Rs.

To test whether the inability of BnOCPA to affect membrane potential was a trivial action due to BnOCPA blocking K⁺ channels mediating the postsynaptic hyperpolarisation, or in some other way non-specifically interfering with G protein signalling, we applied the GABA_B receptor agonist baclofen to CA1 pyramidal neurons. BnOCPA had no effect on membrane

Fig. 1 BnOCPA is an A₁R agonist that discriminates between pre- and postsynaptic A₁Rs in the CNS. **a** Chemical structures of adenosine, CPA and BnOCPA³³. **bi** Schematic representing assays used to characterise the affinity and efficacy of agonists (green arrows) to the human (h) A₁R. **bii** agonist displacement of [³H]DPCPX, a selective antagonist for the hA₁R ($n = 5$ – 10 individual repeats). **biii** cAMP levels measured in CHO-K1-hA₁R cells following co-stimulation with 1 μ M forskolin and each agonist ($n = 4$ – 10 individual repeats). **biv** Both CPA and BnOCPA displace the fluorescent AR agonist NECA-TAMRA in a biphasic manner indicating that both agonists display high affinity and low affinity binding ($n = 4$ individual repeats). **c** Diagram illustrating: left, hippocampal slice preparation showing position of stimulating, patch-clamp and extracellular recording electrodes together with representative electrophysiological recordings: membrane potential (Vm), a fEPSP (field excitatory postsynaptic potential) and seizure activity; right, pre- and postsynaptic A₁Rs at hippocampal synapses and their physiological effects upon activation. **d, e** Increasing concentrations of CPA or BnOCPA reduced the fEPSP, an effect reversed by the A₁R antagonist 8-CPT (2 μ M). Inset, superimposed fEPSP averages in control (largest fEPSP) and becoming smaller with increasing concentrations of CPA or BnOCPA. Scale bars measure 0.2 mV or 0.1 mV and 5 ms for CPA and BnOCPA, respectively. **f, g** Concentration-response curves for the inhibition of synaptic transmission by CPA ($IC_{50} = 11.8 \pm 2.7$ nM; $n = 17$ slices) or BnOCPA ($IC_{50} = 65 \pm 0.3$ nM; $n = 11$ slices). **h** CPA hyperpolarised the membrane potential while BnOCPA had little effect. Scale bars measure 4 mV and 30 s. **i** Summary data for membrane potential changes. The mean hyperpolarisation produced by CPA (300 nM; 7.26 ± 0.86 mV, $n = 7$ cells) was significantly different (one-way ANOVA; $F(2,23) = 70.46$; $P = 1.55 \times 10^{-10}$) from that produced by BnOCPA (300 nM or 1 μ M; 0.33 ± 0.14 mV, $n = 10$ and 5 cells, respectively; $P = 8.26 \times 10^{-11}$) and for CPA (300 nM) applied in the presence of BnOCPA (300 nM; 2.75 ± 0.48 mV, $n = 4$ cells, $P = 2.89 \times 10^{-5}$; See Supplementary Fig. 2a for an example trace). **j** In an in vitro model of seizure activity, represented as frequent spontaneous spiking from baseline, CPA (300 nM) reversibly blocked activity while BnOCPA (300 nM) had little effect. Scale bars measure 0.5 mV and 200 s. **k** Summary data for seizure activity expressed in terms of the frequency of spontaneous spiking before, during and after CPA or BnOCPA. CPA abolished seizure activity ($n = 4$) whereas BnOCPA did not significantly reduce seizure frequency ($n = 6$). Data represented as mean \pm SEM; Two-way RM ANOVA (BnOCPA vs CPA slices): $F(1, 3) = 186.11$, $P = 8.52 \times 10^{-4}$ with the following Bonferroni post hoc comparisons: BnOCPA vs Control; $P = 1$; CPA vs control; $P = 0.010$; BnOCPA vs CPA; $P = 0.027$. Averaged data are presented as mean \pm SEM. ns, not significant; *, $P < 0.05$; **, $P < 0.02$; ****, $P < 0.0001$. Source data are provided as a Source Data file.

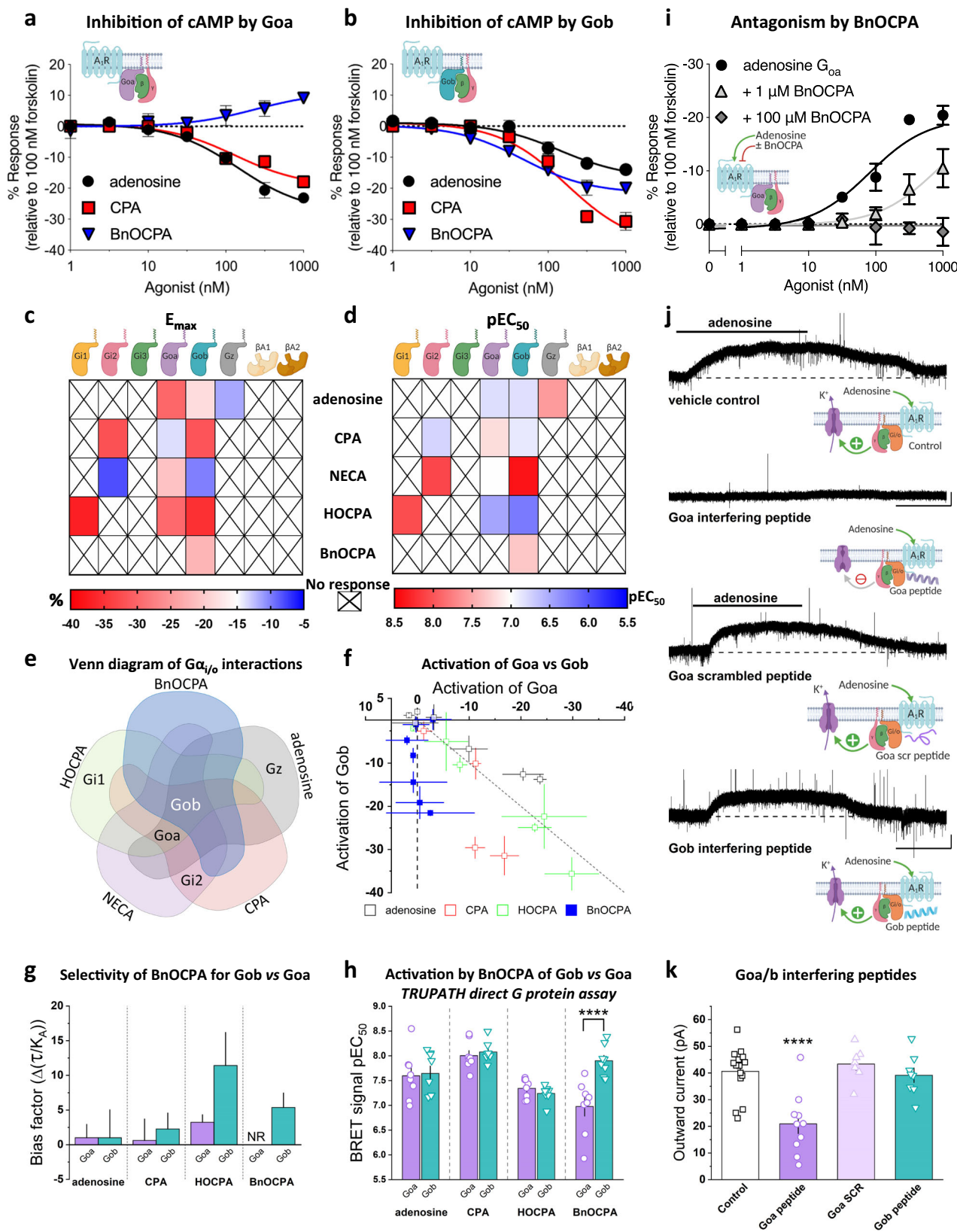
hyperpolarisation produced by baclofen (Supplementary Fig. 2f, g), confirming that the actions of BnOCPA were specific to the A₁R. These observations, of a lack of effect of BnOCPA on postsynaptic membrane potential, likely explained why, in a model of seizure activity, (low Mg²⁺/high K⁺), with prominent postsynaptic depolarisation that promotes neuronal firing, BnOCPA had little effect (Fig. 1j, k). In contrast, equivalent concentrations of CPA completely suppressed neuronal firing (Fig. 1j, k).

BnOCPA demonstrates unique G α signalling in the selective activation of G β . The observation that BnOCPA discriminated between pre- and postsynaptic A₁Rs might be explained if these receptors were to activate different intracellular pathways to mediate their effects, and that BnOCPA was not able to activate the pathway responsible for postsynaptic membrane hyperpolarisation. To test whether the actions of BnOCPA and the prototypical A₁R agonists were mediated via β -arrestins (β -arrestin1 and β -arrestin2), we used a BRET assay^{36–40} for β -arrestin recruitment (Supplementary Fig. 3). We observed no β -arrestin recruitment at the A₁R using either BnOCPA, CPA or adenosine, regardless of whether β -arrestin1 or β -arrestin2 was expressed (Supplementary Fig. 3). This was in contrast to β -arrestin2 recruitment by the A₃R in response to adenosine and NECA, but not BnOCPA (Supplementary Fig. 3). Moreover, the lack of recruitment of β -arrestin1 and β -arrestin2 by the A₁R was independent of any of the six G protein receptor kinase (GRK) isoforms co-expressed with β -arrestin1 and β -arrestin2; only low levels of recruitment were observed even when GRKs were highly (five-fold) overexpressed compared to the levels in the A₃R assays (Supplementary Fig. 4). These observations of a lack of β -arrestin recruitment by A₁Rs are consistent with those previously reported for recombinant A₁Rs expressing native sequences^{41–45}, and are likely due to the absence of serine and threonine residues in the A₁R cytoplasmic tail, which makes the A₁R intrinsically biased against β -arrestin signalling^{19,46}. Accordingly, the differential actions of BnOCPA at pre- and postsynaptic A₁Rs are more likely to reside in selective activation of one G α -mediated pathway over another.

To investigate whether BnOCPA has the ability to discriminate between the various Gai/o subunits activated by adenosine, we

generated a recombinant cell system (CHO-K1 cells) expressing both the hA₁R and individual pertussis toxin (PTX)-insensitive variants of individual Gai/o subunits. Against these individual Gai/o subunits we tested adenosine, CPA, NECA, BnOCPA, and the agonist HOCPA^{33,47}, a stereoisomer of GR79236^{48,49}, which behaved similarly to adenosine and CPA in both inhibiting synaptic transmission and causing membrane hyperpolarisation (Supplementary Fig. 5). In cells treated with PTX to inhibit endogenous Gai/o^{30,33} we observed that adenosine, CPA, NECA and HOCPA activated a range of Gai/o subunits. Common to all of these agonists was the activation of both G α isoforms, G α o and G α b, with differential activation of Gi1 (HOCPA), Gi2 (NECA, CPA) and Gz (adenosine; Fig. 2a–e; Supplementary Figs. 5 and 6). Such promiscuous and biased G α coupling has been described previously for adenosine, CPA, and NECA at recombinant A₁Rs in cell lines^{29,50}, including using novel BRET-based assays for adenosine at some Gai/o⁵¹. These previous observations are in keeping with ours, confirming the validity of the PTX-based approach. In stark contrast, BnOCPA displayed a unique and highly distinctive Gai/o subunit activation profile: BnOCPA was not able to activate Gi1, Gi2, Gi3 or Gz, and was furthermore capable of discriminating between the two G α isoforms via the selective activation of G α b, and not of G α o (Fig. 2a–e; Supplementary Fig. 6).

The selective and unique activation of G α b among the six Gai/o subunits by BnOCPA could be observed in a comparison of the activation of G α o and G α b by the native and selective A₁R agonists in their ability to inhibit the forskolin-stimulated accumulation of cAMP (Fig. 2f). Whereas adenosine, CPA and HOCPA activated both G α o and G α b to inhibit cAMP accumulation, BnOCPA selectively activated G α b, with no discernible activation of G α o. Further quantification of this G α selectivity, through the application of the operational model of receptor agonism^{52–54} to remove potential issues of system bias, confirmed selective activation of G α b by BnOCPA, with no detectable response at G α o (Fig. 2g). As further validation of the ability of BnOCPA to discriminate between the activation of G α o and G α b, we took advantage of BRET assays of GPCR activation^{55,56}, which utilise a reduction in a G α -G β BRET signal to infer agonist-induced G protein activation, including for G α o and G α b⁵⁷ (Fig. 2h; Supplementary Fig. 7a). Using the TRUPATH GPCR BRET assay⁵⁵, adenosine, CPA, and HOCPA



elicited equipotent activation of both Goa and Gob. In stark contrast to these agonists, BnOCPA was >10-fold more efficacious in activating Gob than Goa, and, of all the agonists tested, BnOCPA displayed the weakest potency at Goa. While subtle differences between the Goa and Gob response exist across the two very different in vitro assays, these data nonetheless

confirm that BnOCPA demonstrates a previously unprecedented ability for an A₁R agonist to discriminate between G_α subtypes, and in particular between Goa and Gob.

To establish the functional implications of BnOCPA's profound selectivity for Gob over Goa, we hypothesised that BnOCPA should reduce the actions of adenosine on the

Fig. 2 BnOCPA selectively activates Gob. **a** cAMP accumulation in PTX-pre-treated CHO-K1-hA₁R cells expressing PTX-insensitive Goa following co-stimulation with 1 μM forskolin and each agonist (1 nM–1 μM; *n* = 6 individual repeats). **b** as for **a** but cells were transfected with PTX-insensitive Gob (*n* = 6 individual repeats). Stimulation of cAMP production in **a** reflects BnOCPA's activation of endogenous, PTX-resistant Gs by the A₁R (see Supplementary Figs. 5 and 6 and ^{29,153,154}). **c, d** Heatmaps summarising E_{max} (**c** %) and potency (**d** pEC₅₀; -log [agonist concentration] required for 50% inhibition of cAMP accumulation) for individual Gα subunit and β-arrestin1 and 2 activation by selective A₁R agonists for the inhibition of forskolin-stimulated cAMP production. Data taken from: adenosine, CPA, BnOCPA Fig. 1, Supplementary Figs. 3, 6; NECA, Supplementary Fig. 3, 6; HOCPA, Supplementary Fig. 5. **e** Venn diagram of agonist interactions with individual Gα/i subunits. **f** The inhibition of cAMP accumulation via A₁R:Goa or A₁R:Gob by adenosine, CPA, HOCPA and BnOCPA. Each data point represents a concentration of agonist from the data in Supplementary Figs. 5 and 6. Line of unity (broken grey line) represents no bias. Data presented as mean ± SEM. **g** Signalling bias of A₁R-selective agonists for A₁R-Goa and A₁R-Gob (Δ(τ/KA)) was determined relative to the natural agonist adenosine using the change in (τ/KA) ratio. The values were calculated for all compounds at each individual G protein and the data was fitted globally to determine single values for τ and KA and then normalised to a reference agonist (adenosine). This approach, used by others¹⁵⁵, precludes the provision of individual data points. Compared to adenosine, BnOCPA elicits no measurable response (NR) at Goa. **h** The TRUPATH assay for direct G protein activation reveals no preference between Goa and Gob by adenosine, CPA or HOCPA, but a significant >10-fold greater activation of Gob vs Goa by BnOCPA (two-tailed unpaired Student's t-test; *P* = 0.0009; see also Supplementary Fig. 7a; *n* = 8 individual repeats for each agonist). **i** Adenosine/Goa-mediated inhibition of cAMP accumulation was antagonised by BnOCPA in a concentration-dependent manner (*n* = 3–4 individual repeats). **j** Example current traces produced by adenosine (10 μM) in control conditions or in the presence of intracellular Goa interfering peptide, scrambled Goa peptide or Gob interfering peptide (all at 100 μM). Scale bars measure 25 pA and 100 s. **k** Summary data of adenosine-induced outward current experiments. The mean amplitude of the outward current induced by adenosine (40.6 ± 2.2 pA, *n* = 16 cells) was significantly reduced (one-way ANOVA; *F*(3,37) = 12.40, *P* = 9.22 × 10⁻⁶) to 20.9 ± 3.6 pA (*n* = 10 cells, *P* = 2.65 × 10⁻⁵) in 100 μM Goa interfering peptide. Neither the scrambled Goa peptide (Goa SCR; 43.4 ± 2.4 pA, *n* = 7 cells, *P* = 1) nor the Gob interfering peptide (39.2 ± 2.7 pA, *n* = 8 cells, *P* = 1) reduced the amplitude of the adenosine-induced outward current compared to control, but each were significantly different from the Goa interfering peptide (*P* = 8.20 × 10⁻⁵; *P* = 8.86 × 10⁻⁴, respectively). Averaged data are presented as mean ± SEM. ****, *P* < 0.0001 relative to other groups. Source data are provided as a Source Data file.

inhibition of cAMP accumulation via Goa. This was indeed the case (Fig. 2i): BnOCPA antagonised the Goa-mediated inhibition of cAMP production by adenosine in a concentration-dependent manner. This classic attribute of an antagonist enabled a Schild analysis estimate of BnOCPA's affinity (K_d) to be 113 nM, with a pK_d ~6.9⁵⁸, a value that was quantitatively similar to BnOCPA's ability to bind to the hA₁R (pK_i ~6.6; Fig. 1b). Importantly, this observation, of the ability of BnOCPA to antagonise the actions of adenosine on cAMP inhibition (Fig. 2i), revealed no agonist action of BnOCPA at Goa at concentrations up to 100 μM (>10⁵ greater than the IC₅₀ against cAMP accumulation; Fig. 1b and ~10⁴ greater than the EC₅₀ in the TRUPATH assay; Fig. 2h), and, moreover, had parallels with the antagonising effects of BnOCPA on membrane potential in the CNS (Fig. 1h, i; Supplementary Fig. 2a, c). These data suggest that BnOCPA has the unique ability of displaying both agonist and antagonist-like properties at both recombinant and native A₁R; properties that are expected of a truly Gα subunit-selective agonist.

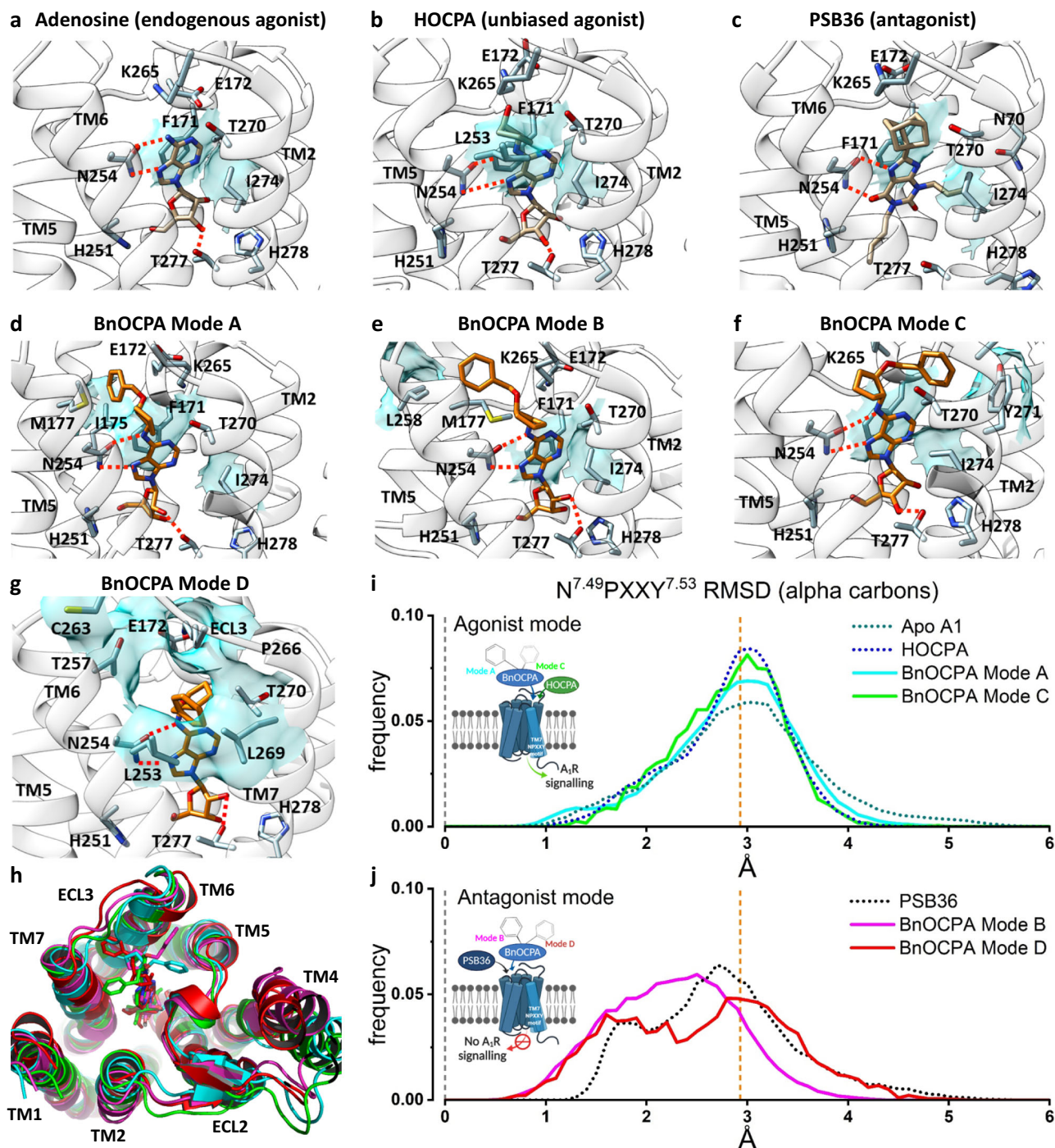
The data from whole-cell patch-clamp recordings showed that BnOCPA did not influence neuronal membrane potential at native A₁R (Fig. 1h, i), while experiments in recombinant hA₁R showed that BnOCPA did not activate Goa (Fig. 2a, c–f), and indeed prevented the activation of Goa by adenosine (Fig. 2i). We thus predicted that A₁R in the hippocampus, where Goa is found at levels 10–15 times higher than Gob⁵⁹, should act via Goa to induce membrane hyperpolarisation, and thereby providing a potential explanation for the lack of effect of BnOCPA on membrane potential. To test this prediction, we injected a series of previously-validated interfering peptides against Goa and Gob^{60–69} into CA1 pyramidal cells during whole-cell voltage-clamp recordings. Introduction of the Goa interfering peptide caused a significant attenuation of the adenosine-induced outward current (Fig. 2j, k). In contrast, neither the scrambled Goa peptide, nor the Gob peptide, which reduced the modulation of Ca²⁺ channels by muscarinic M₄ receptors in striatal cholinergic interneurons⁶³, had any effect on outward current amplitude (Fig. 2j, k). To confirm the specificity and potency of the interfering peptides used in hippocampal neurons, we transfected plasmids coding for the last 11 C-terminal amino acids of either Goa, Gob and the scrambled version of Goa, into

the Goa and Gob vectors in the TRUPATH assay used in Fig. 2h (Supplementary Fig. 7b). The interfering peptides reduced the activation of their cognate G protein in a dose-dependent manner, but had no effect on the alternate Go isoform. The scrambled peptide sequence had no effect on Goa or Gob activation.

Thus, adenosine-mediated membrane potential hyperpolarisation occurs mainly through A₁R activation of Goa, in keeping with the high levels of expression of Goa vs Gob in the hippocampus⁵⁹, and with the observation that the Goa-activating agonists adenosine, CPA and HOCPA (Fig. 2c–e, Supplementary Figs. 5 and 6) all induced membrane hyperpolarisation (Fig. 1h, i; Supplementary Figs. 2 and 5). Moreover, the absence of an effect of adenosine on membrane potential in Gz knockout mice⁷⁰ argues against the possibility that the selective activation of Gz by adenosine observed in our PTX assays (Fig. 2c, d; Supplementary Fig. 6) contributes to membrane hyperpolarisation. The data from recombinant receptors demonstrating the inability of BnOCPA to activate Goa (Fig. 2a, c–g) thus explains why BnOCPA did not cause membrane hyperpolarisation, and indeed prevented or reversed the hyperpolarisation induced by CPA or adenosine, respectively (Fig. 1h, i; Supplementary Fig. 2a, c).

The Ga selectivity displayed by BnOCPA is reflected in non-canonical binding modes and selective interaction with Gai/o subunits.

To better understand the unusual signalling properties of BnOCPA and the highly specific Gα coupling to Gob, we carried out dynamic docking simulations to study the basic orthosteric binding mode of BnOCPA in an explicit, fully flexible environment using the active cryo-EM structure of the A₁R (PDB code 6D9H; Supplementary Movie 1). We previously reported that modifications at position N⁶ of the adenine scaffold modulated the agonist binding path to A₁R⁷¹. More precisely, N⁶-cyclopentyl analogues (CPA and HOCPA) markedly interact with the extracellular loop 2 (ECL2) compared to adenosine, while BnOCPA (which bears the N⁶-cyclopentyl-2-benzyloxy group) is most prone to engage residues of the A₁R located at the top of transmembrane helix 1 (TM1) and TM7. In the present study, we compared the bound-state BnOCPA to the non-Gα selective



agonists adenosine and HOCPA, and an antagonist (PSB36) of the A_1R (Fig. 3a–c). BnOCPA engaged the receptor with the same fingerprint as adenosine⁷² (Fig. 3a) and HOCPA (Fig. 3b, Supplementary Movie 2). Further explorations of the BnOCPA docked state using metadynamics (MetaD) simulations⁷³ revealed interchangeable variations on this fingerprint (namely Modes A, B, and C; Fig. 3d–f; Supplementary Fig. 8) that could be distinguished by the orientation of the BnOCPA-unique benzyl group. Having established the possible BnOCPA binding modes, we examined the respective contribution of the orthosteric agonists, the G protein α subunit $\alpha 5$ (C-terminal) helix (GoCT), and the $G\alpha$ protein subunit^{74,75} to the empirically-observed G protein selectivity displayed by BnOCPA (Fig. 2a–h, Supplementary Fig. 6).

Firstly, following Dror et al.⁷⁶, we compared the dynamics of the BnOCPA-bound A_1R with the corresponding dynamics of the receptor^{77,78} bound to either HOCPA (Fig. 3b), the A_1R antagonist PSB36 (Fig. 3c), or the apo receptor in the absence of G protein, our hypothesis being that there may be ligand-dependent differences in the way that the intracellular region of the receptor responds in the absence of the G protein. In these simulations the G protein was omitted so that inactivation was possible and so that the results were not G protein-dependent. The BnOCPA binding Modes A–C were interchangeable during MD simulations (Table 1) but were associated with distinctly different dynamics, as monitored by changes in a structural hallmark of GPCR activation, the $N^{7.49}PXXY^{7.53}$ motif⁷⁹ (Supplementary Fig. 9). Given the high flexibility shown by the

Fig. 3 Molecular dynamics simulations reveal that BnOCPA binding modes can uniquely drive both agonist- and antagonist-like intracellular conformations of the A₁R.

a Adenosine binding pose: N254^{6,55} (Ballesteros-Weinstein superscript enumeration) is engaged in key hydrogen bonds, while important hydrophobic contacts are shown as cyan transparent surfaces (F171^{ECL2} and I274^{7,39}). **b** On the basis of structural similarities and the dynamic docking (Supplementary Movie 2), HOCPA was predicted to bind with a geometry analogous to adenosine; the cyclopentyl group makes further hydrophobic contacts with L253^{6,54}, as shown by simulation. **c** The xanthine scaffold of the antagonist PSB36 makes hydrogen bonds with N254^{6,55} side chains and hydrophobic contacts with F171^{ECL2} and I274^{7,39}. **d** BnOCPA agonist-like binding Mode A (Supplementary Movie 1): the benzyl group orients towards the ECL2 and makes hydrophobic contacts with I175^{ECL2} (and M177^{5,35}) side chains. **e** BnOCPA antagonist-like binding Mode B: the benzyl group orients towards the top of TM5/TM6 and makes hydrophobic contacts with L258^{6,59} side chain. **f** BnOCPA agonist-like binding Mode C: the benzyl group orients towards the top of TM7 and makes hydrophobic contacts with Y271^{7,36} side chain. **g** Binding orientation of BnOCPA in antagonist-like Mode D: the benzyl group orients under ECL3 and occupies the hydrophobic pocket defined by L253^{6,54}, T257^{6,58}, T270^{7,35}, and L269^{7,34}. Key hydrogen bonds with N254^{6,55} and T277^{7,42} are shown as dotted lines; main hydrophobic contacts are highlighted as cyan transparent surfaces. **h** Extracellular view of the A₁R showing the four BnOCPA binding Modes A (cyan), B (magenta), C (green), and D (red) as randomly extracted from the MD simulations. **i, j** Root-mean-square deviation (RMSD) distributions considering the inactive N^{7,49}PXXY^{7,53} motif on the distal part of TM7 as reference. **i** HOCPA (blue broken line), BnOCPA Mode A (cyan curve), BnOCPA Mode C (green curve) and the apo receptor (dark green broken line) have a common distribution centring around the active conformation of the A₁R (orange broken line; Supplementary Fig. 9) leading to A₁R signalling. In contrast, **j** PSB36 (black broken line), BnOCPA Mode B (magenta curve) and BnOCPA Mode D (red curve) RMSD values have the tendency to move closer to the inactive N^{7,49}PXXY^{7,53} geometry (leftward shift of the curves towards broken grey line at x = 0) preventing A₁R signalling.

BnOCPA benzyl group during the simulations and its lipophilic character, we hypothesised and simulated a further binding mode (namely Mode D) not explored during MD or MetaD simulations. This conformation involves a hydrophobic pocket underneath ECL3 (Fig. 3g) which is responsible for the A₁/A_{2A} selectivity⁷². Superimposition of the four BnOCPA binding Modes A–D reveals the highly motile nature of the benzyl group of BnOCPA (Fig. 3h) under the simulated conditions.

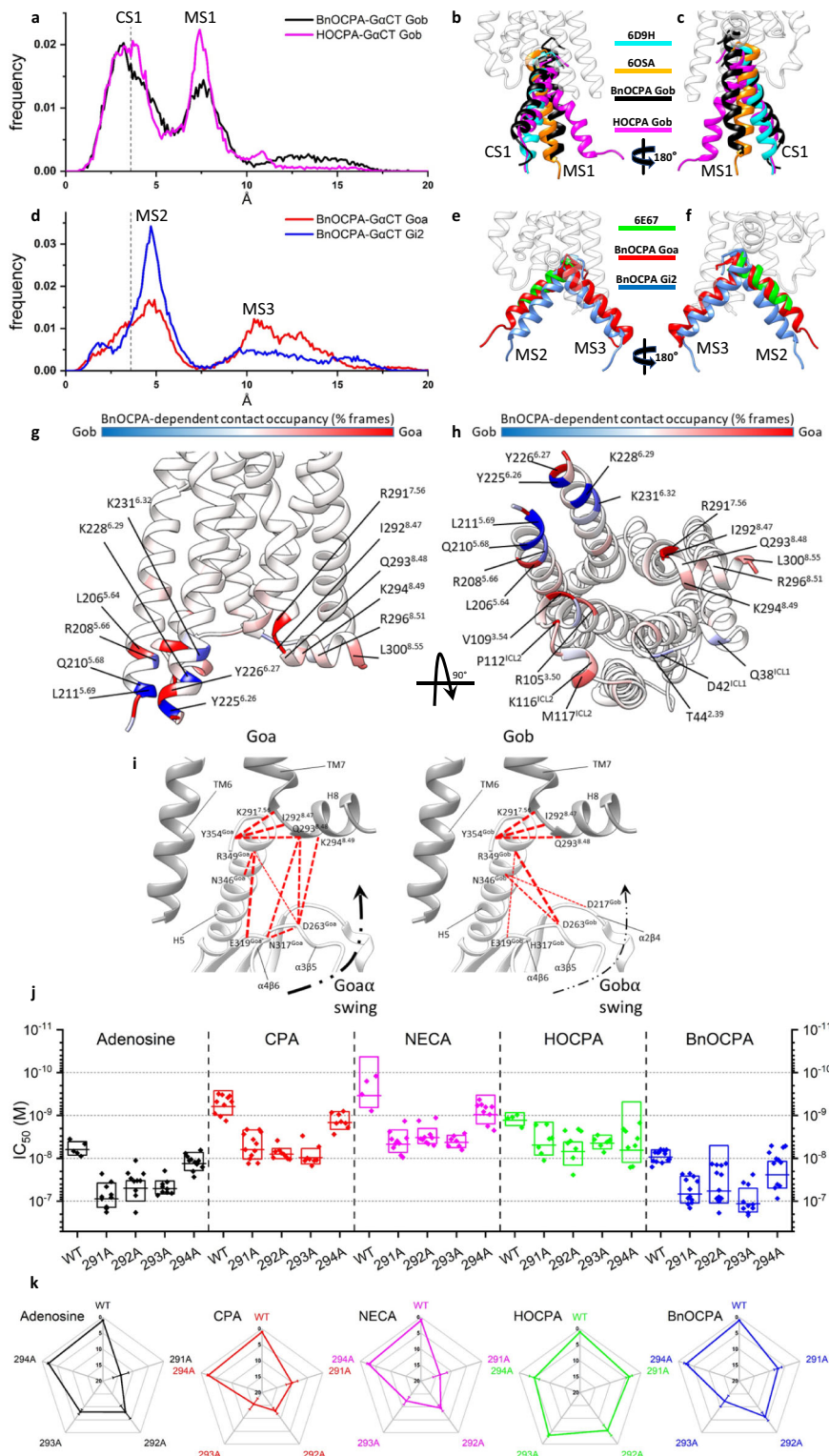
Quantification of the N^{7,49}PXXY^{7,53} dynamics revealed that HOCPA, BnOCPA Mode A, BnOCPA Mode C and the apo receptor show a similar distribution of the RMSD of the conserved N^{7,49}PXXY^{7,53} motif (Fig. 3i; Supplementary Fig. 9). In contrast, the non-canonical BnOCPA binding Modes B and D were responsible for a partial transition of the N^{7,49}PXXY^{7,53} backbone from the active conformation to the inactive conformation (Supplementary Fig. 9) in a manner analogous with the antagonist PSB36 (Fig. 3j). Overall, the simulations revealed Mode D as the most stable BnOCPA pose (6.8 μs out of 9 μs simulated starting from this configuration – Table 1), while Mode B accounted for 3.6 μs out of 30 μs.

Next, to simulate the agonist-driven interaction between the A₁R and the G protein, the α5 (C-terminal) helix (GaCT) of the G protein (Gi2, Goa, Gob) was dynamically docked to the HOCPA- and BnOCPA-bound active A₁R structure (again lacking G protein; Supplementary Movie 3). This allowed us to evaluate the effect of different GaCT on the formation of the complex with A₁R to test the hypothesis that, of Goa, Gob and Gi2, only the GaCT of Gob would fully engage with the BnOCPA-bound active A₁R, in line with the empirical observations of G protein selectivity summarised in Fig. 2c, d. Figure 4a shows that the GaCT of Gob docked to the A₁R via a metastable state (MS1) relative to the canonical state (CS1; Supplementary Movie 3), regardless of whether HOCPA or BnOCPA was bound. Figure 4b, c show that the CS1 geometry corresponds to the canonical arrangement as found in the cryo-EM A₁R:Gi protein complex, whereas state MS1 resembles the recently reported non-canonical state observed in the neurotensin receptor, believed to be an intermediate on the way to the canonical state⁸⁰. In contrast, Fig. 4d–f shows that the GaCT of Goa and Gi2 docks to the A₁R to form metastable states MS2 and MS3. MS2 is similar to the β₂-adrenergic receptor:GsCT fusion complex⁸¹, proposed to be an intermediate on the activation pathway and a structure relevant to G protein specificity. In this case, however, it appears to be on an unproductive pathway.

To test the hypothesis that the non-functional BnOCPA:A₁R:Goa complex showed anomalous dynamics, we next

increased the complexity of the simulations by considering the Ga subunit of the Goa and Gob protein bound to the A₁R:BnOCPA (Mode B or D) complex or the Gob protein bound to A₁R:HOCPA (a functional system). The most visible differences between Goa (Supplementary Movie 4) and Gob (Supplementary Movie 5) comprised the formation of transient hydrogen bonds between the α4–β6 and α3–β5 loops of Goa and helix 8 (H8) of the receptor (Supplementary Table 3). Similar contacts are present in the non-canonical state of the neurotensin receptor:Gi protein complex⁸⁰. Overall, Goa interacted more with TM3 and ICL2 residues (Fig. 4g, h), while TM5 and TM6, along with ICL1, were more engaged by Gob (Fig. 4g, h). Interestingly, R291^{7,56} and I292^{8,47}, which are located under the N^{7,49}PXXY^{7,53} motif, showed a different propensity to interact with Goa or Gob. In this scenario, it is plausible that a particular A₁R conformation stabilised by BnOCPA (as suggested by the simulations in the absence of G protein, Fig. 3i, j) may favour different intermediate states during the activation process of Goa and Gob.

To test the prediction from the MD simulations that R291^{7,56} and I292^{8,47} were involved in A₁R/Ga coupling, we performed a series of site-directed mutagenesis (to alanine) against R291^{7,56}, I292^{8,47} and the adjacent hydrophilic residues Q293^{8,48} and K294^{8,49} (Fig. 4i) and compared the inhibition of forskolin-stimulated cAMP production in response to adenosine, CPA, NECA, HOCPA and BnOCPA in Flp-In-CHO cells against the wild-type (WT) hA₁R (Fig. 4j). Of these residues, none of which are reported to affect binding^{82,83}, K294^{8,49} had the least impact on potency; of the agonists, the mutations had minimal effects on HOCPA. In contrast A₁R/Ga coupling induced by adenosine, CPA, NECA and BnOCPA was affected, but differentially so. These effects on potency (IC₅₀ values) can be readily observed when individual mutant IC₅₀ values are normalised to their respective WT controls (Fig. 4k), and revealed that R291^{7,56}, I292^{8,47} and Q293^{8,48} are especially important for CPA and NECA coupling, R291^{7,56} for adenosine potency, and Q293^{8,48} for BnOCPA. These observations reinforce the MD simulations predictions related to H8 residues involved in G protein coupling of the agonist-stimulated A₁R, and in particular suggest that R291^{7,56}, I292^{8,47} and Q293^{8,48} are especially required for selective agonist coupling to Gα_{o/i}, and may thus contribute to the Ga bias observed among these agonists (Fig. 2c, d). A more detailed analysis, involving saturation mutagenesis of these residues, is required to provide a full characterisation of their actions to direct agonist bias but is beyond the scope of this current study.



BnOCPA does not depress heart rate, blood pressure or respiration: evidence for in vivo physiological selectivity at native A₁Rs. Given BnOCPA’s clear differential effects in a native physiological system (Fig. 1), strong Gob selectivity (Fig. 2), unique binding characteristics (Fig. 3) and selective Gob interaction (Fig. 4), we hypothesised that these properties might circumvent a key obstacle to the development of A₁R agonists for therapeutic use—their powerful effects in the cardiovascular system (CVS) where their activation markedly reduces both heart

rate and blood pressure¹². These cardiovascular effects are likely through Goa, which is expressed at high levels in the heart^{84,85}, particularly in the atria⁸⁶, and which plays an important role in regulating cardiac function⁸⁷. In contrast, and with parallels of differential Goa vs Gob expression in the hippocampus⁵⁹, Gob may be absent or expressed at very low levels in the heart^{86,88}. Given this differential expression of Goa and Gob, and the lack of functional effect of BnOCPA on Goa (Fig. 2a–g), we predicted that BnOCPA would have minimal effects on the CVS. Moreover,

Fig. 4 BnOCPA selectively induces canonical activation states at A₁R:Gob, but non-productive metastable states at other Gαi/o subunits. a–c Dynamic docking of the Gob-GαCT (last 27 residues) performed on the BnOCPA-A₁R (black) and the HOCPA-A₁R (magenta) complex, respectively. **a** Frequency distribution of the RMSD of the last 15 residues of Gob-GαCT (alpha carbon atoms) relative to the Gi2-GαCT conformation reported in the A₁R structure PDB code 6D9H (dashed grey line indicates 3.6 Å resolution). The two most probable RMSD ranges, canonical state (CS) CS1 and metastable state (MS) MS1, can be observed. **b, c** Side views of representative MD frames of the most populated α5 clusters from CS1 and MS1. The last 15 residues of Gob-GαCT in CS1 of both BnOCPA and HOCPA resemble the Gi2-bound state (PDB code 6D9H; cyan). MS1 is characterised by a binding geometry similar to the non-canonical Gi intermediate state reported for the neurotensin receptor structure (PDB Code 6O5A; orange). **d–f** Dynamic docking of the Goa- and Gi2-GαCT (last 27 residues) performed on the BnOCPA-A₁R complex. **d** As for **a** except Gob was replaced with Goa (red) and compared to Gi2 (blue), with the two most probable RMSD ranges labelled as MS2 and MS3. **e, f** Side views of representative MD frames of the most populated GαCT clusters from MS2 and MS3. The Goa and Gi2 last 15 residues in MS2 overlap well with the putative Gs intermediate state (PDB code 6E67; green). In MS3, the GαCT helix orients in unique conformations that differ from those previously described. **g, h** For each residue the interaction plotted on the backbone is the difference between the Goa and Gob occupancies in the presence of orthosteric BnOCPA (% of MD frames in which interaction occurred). BnOCPA/A₁R/Goa (inactive coupling) had the tendency to interact more with ICL2, TM3 TM7, and H8 (red), while BnOCPA/A₁R/Gob (active coupling) formed more contacts with TM5 and TM6 (blue). **i** Residues in TM7 and H8 of the hA₁R predicted by MD simulations to be of importance to A₁R coupling to Goa (left) and Gob (right). **j, k** Mutations of R291^{7.56}, I292^{8.47}, Q293^{8.48} and K294^{8.49} to alanine in the hA₁R differentially affect agonist efficacy against stimulated cAMP production. **j** Data points represent individual IC₅₀ values (n = 5–13 individual experiments), with the mean represented as the horizontal bar and the box limits indicating ±1 SD. **k** Spider plot summarising data from **j**. Source data are provided as a Source Data file.

given the antagonism of Goa-mediated actions by BnOCPA at native and recombinant A₁Rs (Fig. 1h, i, Supplementary Fig. 2a, c, Fig. 2i), we further predicted that the actions of adenosine on the CVS may be attenuated by BnOCPA.

In initial experiments, we screened BnOCPA for its effects on heart rate using an isolated frog heart preparation. In contrast to adenosine and CPA, which depress heart rate through hyperpolarisation caused by activation of cardiac sinoatrial K⁺ channels⁸⁹, BnOCPA had no effect on heart rate, but markedly reduced the bradycardia evoked by adenosine (Supplementary Fig. 10a). Thus, BnOCPA appears not to activate A₁Rs in the heart, but instead behaves like an antagonist in preventing the actions of the endogenous agonist. These observations have parallels with BnOCPA's inability to activate A₁Rs to hyperpolarise neurones, and indeed inhibiting or reversing the post-synaptic hyperpolarisation induced by typical A₁R agonists (Fig. 1h, i; Supplementary Fig. 2a, c), and in preventing the A₁R/Goa-mediated inhibition of cAMP accumulation by adenosine (Fig. 2i). Such antagonist-like behaviour may be explained by BnOCPA causing unique A₁R conformations unlike those of conventional agonists (Fig. 3i, j), and driving non-canonical and ultimately non-productive interactions with Goa (Fig. 4).

To investigate the effects of BnOCPA in an intact mammalian system, we measured the influence of BnOCPA on heart rate and blood pressure in urethane-anaesthetised, spontaneously breathing adult rats. As expected, both resting heart rate and arterial blood pressure were significantly reduced by adenosine and CPA (Fig. 5a–d). In complete contrast, BnOCPA had no effect on either heart rate (Fig. 5a, c) or blood pressure (Fig. 5b, d), even when applied at two or three times the initial dose (Supplementary Fig. 11; Fig. 6e, f). These negative observations could not be explained by metabolism of BnOCPA to an inactive substance since BnOCPA is a very stable compound (half-life ($t_{1/2}$) >240 min in PBS at 37 °C) with a human plasma stability of ~100% remaining after 120 mins suggesting a $t_{1/2}$ > 240 min at 37 °C. In addition, the *in vitro* metabolic $t_{1/2}$ of BnOCPA was determined as >60 mins using human liver microsomes (0.1 mg/mL, 37 °C), and the intrinsic clearance (CL_{int}) calculated as <115.5 μL/min/mg. This was in contrast to the reference compounds verapamil and terfenadine (0.1 μM) with $t_{1/2}$ in human plasma determined as 33 and 10 min and CL_{int} as 213.1 and 683.0 μL/min/mg, respectively (see Supporting Data File 1). Further evidence that BnOCPA was present and active during these experiments was obtained from studies analogous to those in frog heart when BnOCPA was applied together with adenosine. In the intact anaesthetised rat, when co-applied with adenosine or

CPA, BnOCPA abolished the bradycardia induced by both agonists, indicating its ability to bind to the A₁R at the dose applied (Fig. 5a, c; Fig. 6g, Supplementary Figs. 10b and 11). Volumes of saline equivalent to the drug injections had no effect on either heart rate or blood pressure and there was no waning in the effects of adenosine responses with repeated doses (Supplementary Fig. 10c, d). Thus, BnOCPA does not appear to act as an agonist at CVS A₁Rs, but instead antagonises the bradycardic effects of A₁R activation on the heart.

Since adverse effects on respiration (dyspnoea) limit the use of systemic A₁R agonists⁷, we additionally examined the effects of BnOCPA on respiration. In urethane-anaesthetised, spontaneously breathing adult rats, intravenous injection of BnOCPA had no appreciable effect on respiration (Fig. 6a–d), even if the dose of BnOCPA was doubled or trebled (Fig. 6e, f). In stark contrast the selective A₁R agonist CPA caused significant respiratory depression (Fig. 6a–d). Paralleling BnOCPA's antagonism of adenosine- and CPA-induced depressions of heart rate (Fig. 5a, c; Supplementary Figs. 10b and 11), BnOCPA reduced the depression of respiratory frequency and minute ventilation caused by CPA (Fig. 6g, Supplementary Fig. 11). These data suggest that while BnOCPA targets and clearly engages the A₁Rs responsible for adenosine and CPA's cardiorespiratory depression, BnOCPA has no agonist action at these A₁Rs.

BnOCPA is a potent analgesic. Our observations of a lack of effect of BnOCPA on the CVS and respiration prompted an investigation into a potential application of A₁R agonists that had previously been severely curtailed by adverse cardiorespiratory events^{7,16}, namely the use of A₁R agonists as analgesics. Since sedation or motor impairment can be mistaken for analgesia, we tested BnOCPA in a sensitive assay for balance and motor coordination, the rotarod, in which the ability of a rodent to remain upon a slowly accelerating rotating cylinder is a measure of alertness and motor function. As a positive control for the sensitivity of the test, we showed that the ability of animals treated with morphine to remain on the rotating cylinder was strongly impaired (Fig. 7a). In contrast, the performance of animals treated with BnOCPA, delivered either intravenously or intraperitoneally, was indistinguishable from vehicle-treated mice (Fig. 7a). This was true even if BnOCPA was injected intravenously at three times the dose (Fig. 7a), which, while having no cardiorespiratory actions on its own, prevented cardiorespiratory depression caused by adenosine and CPA (Figs. 5 and 6; Supplementary Figs. 10 and 11). Thus, BnOCPA does not induce

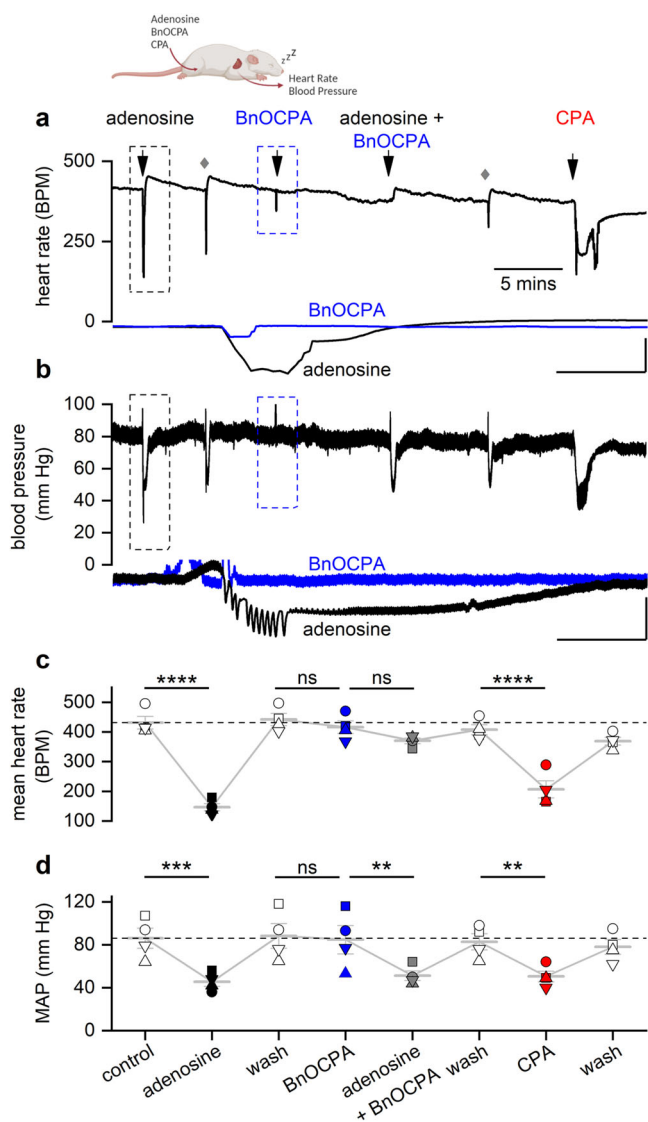


Fig. 5 BnOCPA does not affect heart rate or blood pressure. **a** Examples of heart rate (HR) and **b** arterial blood pressure traces from a urethane-anesthetized, spontaneously breathing rat showing the effects of adenosine (1 mg kg^{-1}), BnOCPA ($8 \text{ } \mu\text{g kg}^{-1}$) and CPA ($6 \text{ } \mu\text{g kg}^{-1}$). Grey diamonds reflect saline flushing of the femoral vein catheter. Insets are expanded HR and blood pressure responses to adenosine and BnOCPA (black and blue traces, respectively; boxed regions in **a** and **b**). Scale bars measure: HR, 200 BPM and 6 s; blood pressure, 40 mm Hg and 6 s. **c, d** Summary data for 4 rats where each rat is shown as a different symbol with the means (\pm SEM, light grey bars) connected. One-way RM ANOVA for: **c** HR, Greenhouse-Geisser corrected $F(2.33, 7.00) = 68.27$, $P = 2.07 \times 10^{-5}$; **d** mean arterial blood pressure (MAP), Greenhouse-Geisser corrected $F(1.84, 5.52) = 10.51$, $P = 0.014$; with the following Bonferroni post hoc comparisons: The resting HR of 432 ± 21 BPM was significantly reduced to 147 ± 12 BPM (-66% , $P = 2.76 \times 10^{-11}$) by adenosine. BnOCPA had no effect on HR (-6% , 442 ± 20 vs 416 ± 21 BPM; $P = 1$) but prevented the bradycardic effects of adenosine ($P = 2.71 \times 10^{-9}$ vs adenosine) when co-injected (mean change 51 ± 4 BPM; -12% ; $P = 0.67$). CPA significantly decreased HR (from 408 ± 17 to 207 ± 29 BPM; -50% , $P = 1.85 \times 10^{-8}$), a decrease that was not different to the effect of adenosine ($P = 0.12$), but was significantly different to the effect of both BnOCPA ($P = 9.00 \times 10^{-9}$) and adenosine in the presence of BnOCPA ($P = 6.69 \times 10^{-7}$). The resting MAP (86 ± 9 mm Hg) was significantly reduced by adenosine (-47% , 46 ± 4 mm Hg; $P = 0.001$). BnOCPA had no effect on its own on MAP (88 ± 11 vs 85 ± 13 mm Hg; $P = 1$) and did not prevent adenosine in lowering MAP to a value similar to adenosine on its own (51 ± 4 mm Hg; $P = 1$ vs adenosine; $P = 0.012$ vs BnOCPA alone). CPA significantly decreased MAP (from 83 ± 8 to 51 ± 5 mm Hg; $P = 0.017$), a decrease that was not different to the effect of adenosine in the absence or presence of BnOCPA ($P = 1$ for both). ns, not significant; **, $P < 0.02$; ***, $P < 0.001$; ****, $P < 0.0001$. Source data are provided as a Source Data file.

sedation or locomotor impairment that could confound interpretations of analgesia.

To assess the potential of BnOCPA as an analgesic, we used a rat model of chronic neuropathic pain (spinal nerve ligation)⁹⁰ a feature of which is mechanical allodynia whereby the affected limb is rendered sensitive to previously innocuous tactile stimuli, and which models the debilitating human clinical condition of chronic pain, which affects between 20 and 50% of the population^{91,92}, and which carries a major global burden of disability⁹³.

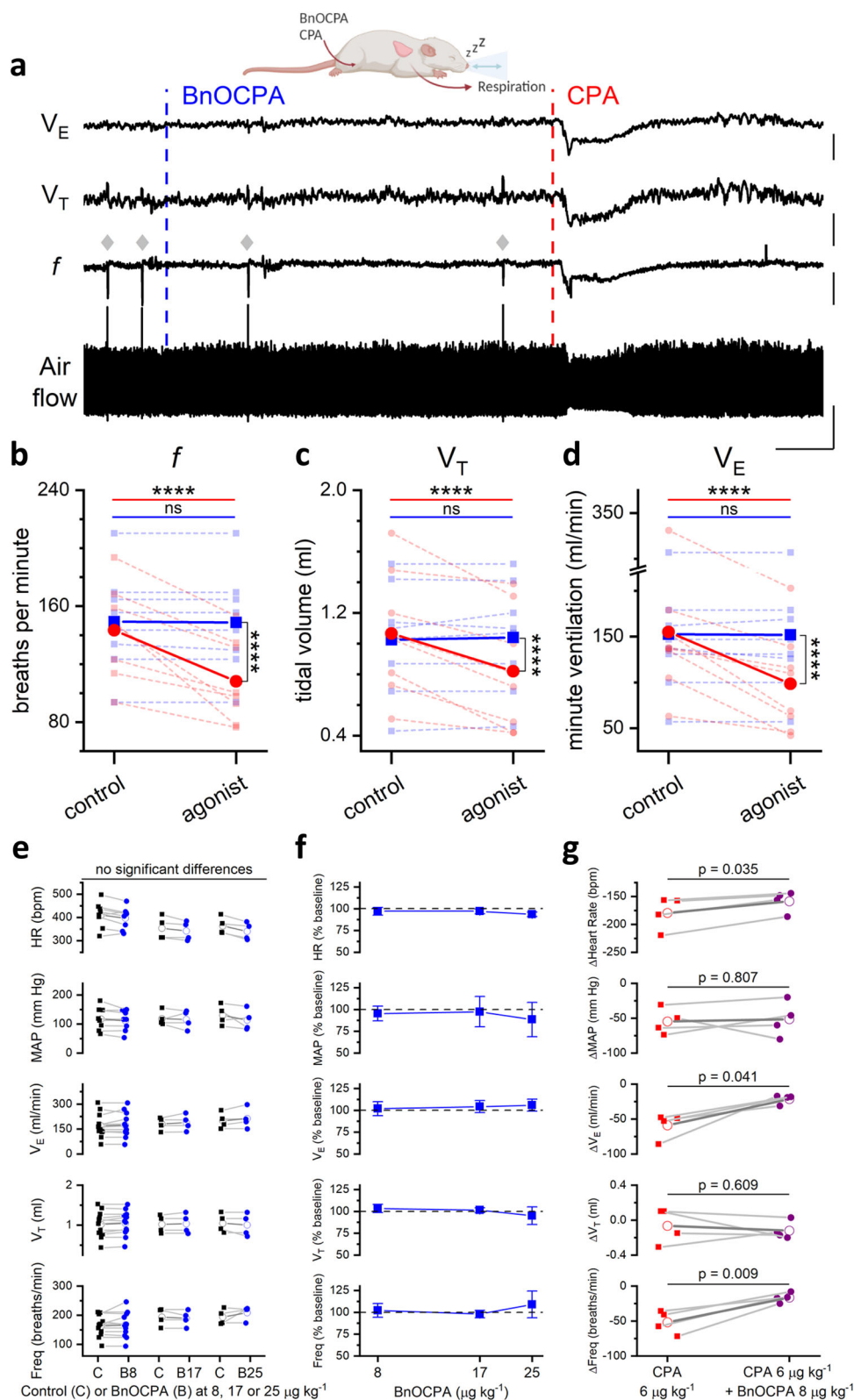
Both intrathecal (Fig. 7b) and intravenous (Fig. 7c) BnOCPA potently reversed mechanical allodynia in a dose-dependent manner. Thus, BnOCPA exhibits powerful analgesic properties at doses devoid of sedative or cardiorespiratory effects, and at several orders of magnitude lower than the non-opioid analgesics pregabalin and gabapentin⁹⁴. To test if this analgesia was mediated by the activation of A_1 Rs by BnOCPA, we used the selective A_1 R antagonist, DPCPX. Prior administration of DPCPX prevented the reversal of mechanical allodynia by BnOCPA (Fig. 7d), confirming the importance of A_1 Rs in mediating the analgesic actions of BnOCPA. In contrast, the rat A_3 R-selective antagonist MRS1523^{95,96}, which is effective in reversing analgesia caused by selective A_3 R agonists^{97–99}, had no effect on the analgesia caused by BnOCPA, and indeed may have provoked a slight facilitation. This may be due to the reported

elevated adenosine tone¹⁰⁰ and activation of A_3 Rs¹⁰¹ in the neuropathic spinal cord, which may have resulted in the desensitisation of A_1 R-mediated responses¹⁰². These observations confirm that the analgesia provoked by BnOCPA is mediated via the selective activation of A_1 Rs.

Discussion

Biased agonists at GPCRs offer great potential for the preferential activation of desirable intracellular signalling pathways, while avoiding, or indeed blocking those pathways that lead to adverse or unwanted effects^{3,27}. While this, and the potential to exploit previously unattractive drug targets such as the A_1 R, have been appreciated, translation of in vitro observations, particularly of G_{α} bias, to native receptors in vivo has been problematic^{3,4,27}. Here we have shown that translation of in vitro selectivity among G_{α} subunits, identified using two separate assays, to an intact physiological system is possible through a benzyloxy derivative (BnOCPA) of the selective A_1 R agonist CPA. Moreover, this G_{α} selectivity has occurred in the context of the A_1 R, an attractive, but notoriously intractable drug target by virtue of the profound cardiorespiratory consequences of its activation by conventional A_1 R agonists.

BnOCPA was first reported as a final compound in a patent where it was described to be selective for the A_1 R with respect to its binding affinity, and effective in reducing elevated intraocular pressure for the potential treatment of glaucoma or ocular hypertension³⁴. We have previously prepared BnOCPA (and HOCPA)³³ for assessment as part of our synthetic campaign to develop potent and A_1 R-selective fluorescent ligands. The N^6 -substituent (1*R*,2*R*)-2-aminocyclopentan-1-ol present in BnOCPA and HOCPA is also found in the experimental and later discontinued¹⁰³ drug CVT-3619 (later named GS 9667), which



has been described as a partial, selective agonist of the A_1R and shown to reduce cAMP content and lipolysis in rat adipocytes¹⁰⁴.

Having identified BnOCPA as a selective G_{ob} agonist at recombinant A_1R s in vitro, we established that this unusual property can be translated into the selective activation of native A_1R s in both the in vitro CNS and in vivo cardiorespiratory and peripheral nervous systems. Moreover, these properties of

BnOCPA were observed at A_1R s expressed by three different species: amphibian, rat, and human. While BnOCPA bound to and induced A_1R coupling to $G_{\text{ai/o}}$ subunits recruited by prototypical A_1R agonists such as adenosine and CPA, BnOCPA selectively activated G_{ob} among the six $G_{\text{ai/o}}$ subunits. This likely reflected BnOCPA's non-canonical binding profile at the A_1R , which had profound implications for the interaction with the

Fig. 6 BnOCPA does not cause respiratory depression. **a** Examples of tracheal airflow, respiratory frequency (f), tidal volume (V_T) and minute ventilation (V_E) from a urethane-anaesthetised, spontaneously breathing rat showing the lack of effect of BnOCPA on respiration and the respiratory depression caused by CPA. BnOCPA or CPA were given intravenously at the times indicated by the vertical broken lines (BnOCPA, $8 \mu\text{g kg}^{-1}$, blue; CPA, $6 \mu\text{g kg}^{-1}$, red). Grey diamonds indicate spontaneous sighs. Scale bars measure: 180 s and: airflow, 0.5 mL; f , 50 breaths per minute (BrPM); V_T , 0.25 mL; V_E , 50 mL/min. **b–d** Summary data for 8 animals. Data from each rat is shown before and after the injection of BnOCPA (blue squares and broken lines) or CPA (red circles and broken lines) together with the mean value for all animals (solid lines) for f , V_T and V_E , respectively. One-way RM ANOVA: For: **b** f , Greenhouse-Geisser corrected $F(1.20, 8.38) = 30.4$, $P = 3.48 \times 10^{-4}$; **c** V_T , $F(3, 21) = 15.9$, $P = 1.25 \times 10^{-5}$, and **d** V_E , Greenhouse-Geisser corrected $F(1.19, 8.34) = 15.77$, $P = 0.003$, with the following Bonferroni post hoc comparisons: Following BnOCPA, f (149 ± 12 BrPM), V_T (1.0 ± 0.1 mL), and V_E (152 ± 26 mL/min) were not altered ($P = 1$) compared to resting values f (149 ± 12 BrPM), V_T (1.0 ± 0.1 mL), and V_E (153 ± 26). In contrast to CPA, which reduced f (108 ± 10 BrPM), V_T (0.8 ± 0.1 mL), and V_E (99 ± 19 mL/min) compared to resting values f (143 ± 11 BrPM; $p = 4.05 \times 10^{-6}$), V_T (1.1 ± 0.1 mL; $P = 2.58 \times 10^{-5}$), and V_E (155 ± 28 ; $P = 5.52 \times 10^{-5}$). The control resting values before administration of BnOCPA and CPA were not different to one another ($P = 1$). The effects of CPA were significantly greater than BnOCPA for f ($P = 4.48 \times 10^{-7}$), V_T ($P = 1.15 \times 10^{-4}$), and V_E ($P = 1.16 \times 10^{-4}$). Horizontal significance indicators above the data show differences between resting values and following IV administration of either BnOCPA (blue line) or CPA (red line). Vertical significance indicators show differences between the effects of BnOCPA and CPA. **e** Individual data ($n = 4$ –12 rats) for the three doses of BnOCPA (blue circles) compared to their preceding baseline (black squares). The mean is shown as an open symbol. One-way ANOVA with Bonferroni corrections found no differences in: HR ($p = 0.07$), MAP ($p = 1$), Freq ($P = 0.2$), V_T ($p = 1$), or V_E ($p = 0.9$). **f** Average data from the animals in **e** showing cardiorespiratory variables as a percentage of their preceding baseline and as a function of increasing dose of BnOCPA (\log_{10} scale). **g** Individual data from four rats showing the effect (difference from the previous baseline) of CPA in the absence (red squares) and presence (purple circles) of BnOCPA ($8 \mu\text{g kg}^{-1}$). The mean is shown as an open symbol. Two-tailed paired t-tests indicated a significant reduction in the effects of CPA by BnOCPA on: HR (CPA: 179 ± 15 bpm vs BnOCPA: 159 ± 10 bpm; $p = 0.035$), V_E (CPA: 59 ± 9 mL/min vs BnOCPA: 21 ± 3 mL/min; $p = 0.041$) and Freq (CPA: 52 ± 8 breaths/min vs BnOCPA: 17 ± 3 breaths/min; $p = 0.009$), with no change in: MAP ($p = 0.807$) or V_T ($p = 0.609$). Data are shown as mean \pm SEM. Raw traces from a representative experiment can be found in Supplementary Fig. 11. Source data are provided as a Source Data file.

G α CT in terms of different binding pathways and intermediate states, and in the different intra- and intermolecular hydrogen bond patterns and contacts observed in the simulations of the A $_1$ R in complex with either Goa (inactive) or Gob (active). Predictions from the MD simulations suggested four hitherto uncharacterised residues as being important for the interaction between the A $_1$ R and Gai/o. Individual mutations in three of these contacts, R291^{7,56}, I292^{8,47}, Q293^{8,48}, differentially impacted agonist efficacy, with adenosine and HOCPA being relatively unaffected compared to the stronger effects on the efficacy of CPA, NECA and BnOCPA. These and other molecular differences in the coupling of the A $_1$ R to Gai/o are likely to underlie the ability of the BnOCPA-bound A $_1$ R to selectively trigger Gob activation among the six Gai/o subtypes.

The unique and unprecedented G α selectivity displayed by BnOCPA has physiological importance since it is able to inhibit excitatory synaptic transmission without causing neuronal membrane hyperpolarisation, sedation, bradycardia, hypotension or dyspnoea. BnOCPA thus overcomes cardiovascular and respiratory obstacles to the development of adenosine-based therapeutics that have plagued the field since their first description nine decades ago¹⁰⁵. As a first, but significant, step towards this, we demonstrate that BnOCPA has powerful analgesic properties via A $_1$ Rs in an in vivo model of chronic neuropathic pain, potentially through a mechanism that may involve a combination of inhibition of synaptic transmission in peripheral and spinal pain pathways, and the hyperpolarisation of Gob-containing nociceptive neurons. Chronic pain, a condition that a large proportion of the population suffers on a constant or frequent basis^{91,92} and associated with a major global burden of disability⁹³ is, however, a disorder for which the current treatments are either severely lacking in efficacy¹⁰⁶ or, in the case of opioids, come with unacceptable harms such as adverse gastrointestinal effects, respiratory depression, tolerance, dependence and abuse potential¹⁰⁷. Accordingly, novel treatments for chronic pain are urgently required.

We have shown that highly selective G α agonism in vitro can be translated into selective activation of native A $_1$ Rs to mediate differential physiological effects, and have identified a novel molecule capable of doing so. We have also explored molecular mechanisms by which this could occur, and demonstrated pain as

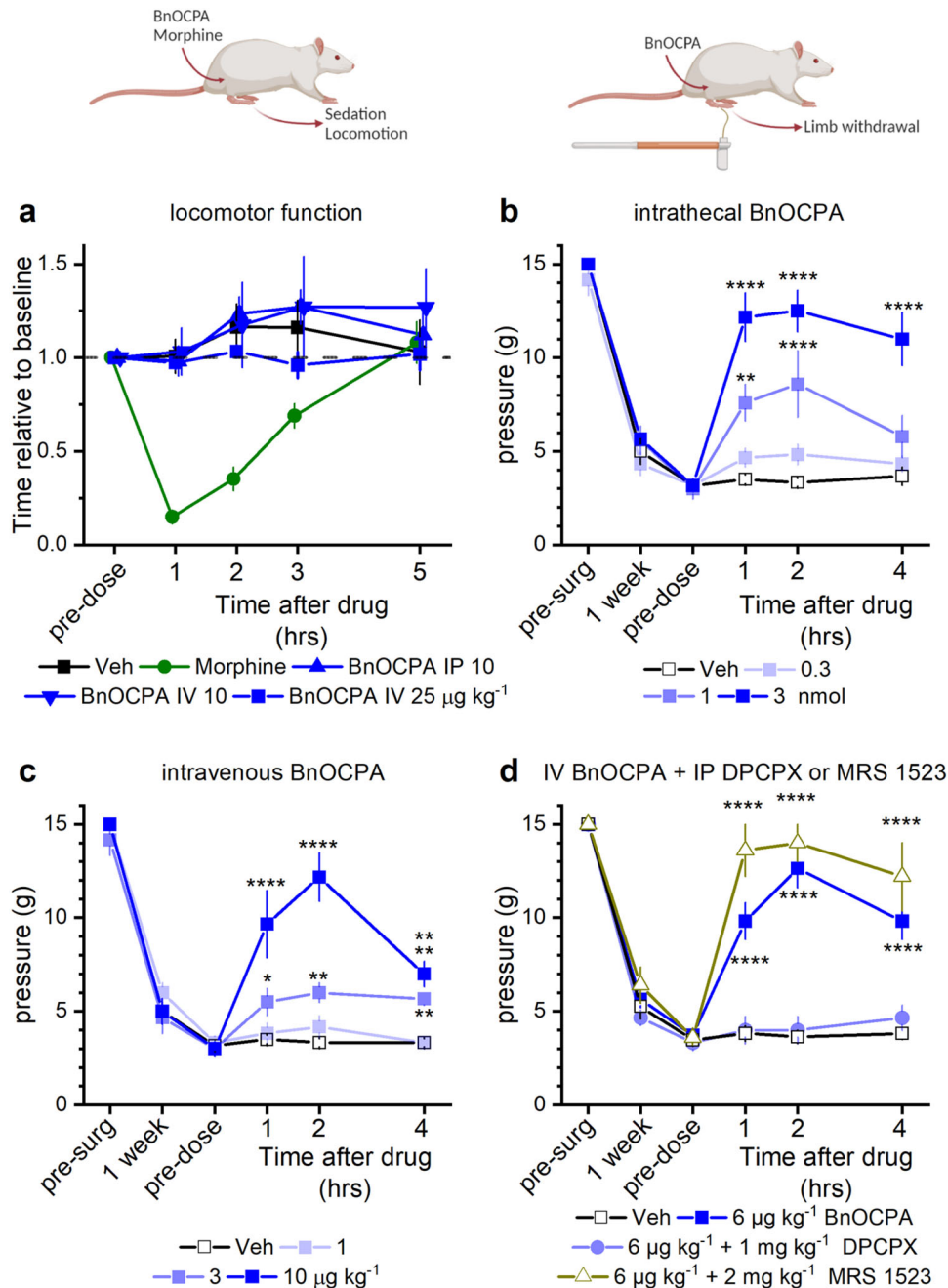
one potential and wide-reaching therapeutic application. Such discoveries are of importance in both understanding GPCR-mediated signalling, and in the generation of both new research tools and therapeutics based on the untapped potential of biased, and indeed G α -selective, agonists such as BnOCPA.

Methods

Approvals. All experiments involving animals were conducted with the knowledge and approval of the University of Warwick Animal Welfare and Ethical Review Board, and in accordance with the U.K. Animals (Scientific Procedures) Act (1986) and the EU Directive 2010/63/EU. In vivo cardiorespiratory studies were conducted under the auspices of UK PPL 70/8936 and chronic neuropathic pain studies under the auspices of P9D9428A9. Rotarod studies were approved by the Monash University Animal Ethics Committee in accordance with the Australian Code for the Care and Use of Animals for Scientific Purposes (2013) under Monash AEC protocol number 13333.

Preparation of hippocampal slices. Sagittal slices of hippocampus (300–400 μm) were prepared from male Sprague–Dawley rats, at postnatal days 12–20¹⁰⁸. Rats were kept on a 12-hour light–dark cycle with slices made 90 min after entering the light cycle. In accordance with the U.K. Animals (Scientific Procedures) Act (1986), rats were killed by cervical dislocation and then decapitated. The brain was removed, cut down the midline and the two sides of the brain stuck down to a metal base plate using cyanoacrylate glue. Slices were cut along the midline with a Micro HM 650 V microslicer in cold (2–4 °C), high Mg²⁺, low Ca²⁺ artificial cerebrospinal fluid (aCSF), composed of (mM): 127 NaCl, 1.9 KCl, 8 MgCl₂, 0.5 CaCl₂, 1.2 KH₂PO₄, 26 NaHCO₃, 10 D-glucose (pH 7.4 when bubbled with 95% O₂ and 5% CO₂, 300 mOSM). Slices were stored at 34 °C for 1–6 h in aCSF (1 mM MgCl₂, 2 mM CaCl₂) before use.

Extracellular recording. A slice was transferred to the recording chamber, submerged in aCSF and perfused at 4–6 mL min⁻¹ (32 ± 0.5 °C). The slice was placed on a grid allowing perfusion above and below the tissue and all tubing was gassed (to prevent loss of oxygen). An aCSF-filled glass microelectrode was placed within stratum radiatum in area CA1 and recordings were made using either a differential model 3000 amplifier (AM systems, WA USA) or a DP-301 differential amplifier (Warner Instruments, Hampden, CT USA). Field excitatory postsynaptic potentials (fEPSPs) were evoked with either an isolated pulse stimulator model 2100 (AM Systems, WA) or ISO-Flex (AMPI, Jerusalem, Israel). For fEPSPs a 10–20 min baseline was recorded at a stimulus intensity that gave 40–50% of the maximal response. Signals were acquired at 10 kHz, filtered at 3 kHz, and digitised on line (10 kHz) with a Micro CED (Mark 2) interface controlled by Spike software (Vs 6.1, Cambridge Electronic Design, Cambridge UK) or with WinLTP¹⁰⁹. For fEPSP slope, a 1 ms linear region after the fibre volley was measured. Extracellular recordings were made independently on two electrophysiology rigs. As the data obtained from each rig was comparable, both sets of data have been pooled.



Seizure model. Seizure activity was induced in hippocampal slices using nominally Mg^{2+} -free aCSF that contained no added Mg^{2+} and with the total K^{+} concentration increased to 6 mM with KCl. Removal of extracellular Mg^{2+} facilitates depolarisation via glutamate N-methyl-D-aspartate (NMDA) receptor activation. Increasing the extracellular concentration of K^{+} depolarises neurons leading to firing and release of glutamate to sustain activity. Both the increase in K^{+} concentration and removal of Mg^{2+} are required to produce spontaneous activity in hippocampal slices¹¹⁰. Spontaneous activity was measured with an aCSF-filled microelectrode placed within stratum radiatum in area CA1.

Whole-cell patch-clamp recording from hippocampal pyramidal cells. A slice was transferred to the recording chamber and perfused at 3 ml min^{-1} with aCSF at 32 ± 0.5 °C. Slices were visualised using IR-DIC optics with an Olympus BX151W microscope (Scientifica) and a CCD camera (Hitachi). Whole-cell current- and voltage-clamp recordings were made from pyramidal cells in area CA1 of the hippocampus using patch pipettes (5–10 M Ω) manufactured from thick walled glass (Harvard Apparatus, Edenbridge UK) and containing (mM): potassium gluconate 135, NaCl 7, HEPES 10, EGTA 0.5, phosphocreatine 10, MgATP 2, NaGTP 0.3 and biocytin 1 mg ml^{-1} (290 mOSM, pH 7.2). Voltage and current recordings were obtained using an Axon Multiclamp 700B amplifier (Molecular Devices, USA) and digitised at 20 KHz. Data acquisition and analysis was

performed using pClamp 10 (Molecular Devices, USA). For voltage-clamp experiments, CA1 pyramidal cells were held at -60 mV. Peptides to interfere with G protein signalling were introduced via the patch pipette into the recorded cell. The cell was held for at least 10 min before adenosine (10 μM) was added to induce an outward current.

Frog heart preparation. Young adult male *Xenopus leavis* frogs were obtained from Portsmouth Xenopus Resource Centre. Frogs were euthanized with MS222 (0.2% at a pH of 7), decapitated and pithed. The animals were dissected to reveal the heart and the pericardium was carefully removed. Heart contractions were measured with a force transducer (AD instruments). Heart rate was acquired via a PowerLab 26 T (AD instruments) controlled by LabChart 7 (AD instruments). The heart was regularly washed with Ringer solution and drugs were applied directly to the heart.

In vivo anaesthetised rat preparation for cardiorespiratory recordings. Anaesthesia was induced in adult male Sprague-Dawley rats (230–330 g) with isofluorane (2–4%; Piramal Healthcare). The femoral vein was catheterised for drug delivery. Anaesthesia was maintained with urethane (1.2–1.7 g kg^{-1} ; Sigma) in sterile saline delivered via the femoral vein catheter. Body temperature was

Fig. 7 BnOCPA is a potent analgesic without causing sedation or motor impairment. **a** BnOCPA did not induce sedation or affect motor function when injected intraperitoneally (IP; $10 \mu\text{g kg}^{-1}$) or intravenously (IV; 10 or $25 \mu\text{g kg}^{-1}$). In contrast, morphine caused sedation and motor impairment (15 mg kg^{-1} subcutaneously, SC). Saline (Veh, SC) did not affect rotarod performance. Data points (mean \pm SEM; $n = 6$ for each compound) are normalised to pre-dose performance and are offset for clarity. **b, c** BnOCPA alleviates mechanical allodynia in neuropathic pain when administered **b** via an intrathecal (IT) or **c** IV route. Pre-surgery (pre-surg) animals had similar sensitivity to tactile stimulation as assessed by von Frey hair stimulation. Spinal nerve ligation caused hypersensitivity to touch (mechanical allodynia) at 1 week after surgery as evidenced by the reduction in the tactile pressure necessary to elicit paw withdrawal (paw withdrawal threshold; PWT). PWT reaches a similar nadir across all groups prior to the vehicle or BnOCPA infusion (pre-dose). Administration of BnOCPA significantly increased PWT in the limb ipsilateral to the site of injury in a dose-dependent manner (one-way ANOVA (pre-dose, 1, 2 and 4 hrs) for IT BnOCPA $F(3,88) = 21.9$, $P = 1.10 \times 10^{-10}$; for IV BnOCPA $F(3,92) = 18.1$, $P = 2.70 \times 10^{-9}$). Fisher LSD post hoc comparisons showed significant differences at: IT 1 nmol at 1 and 2 hrs, $P = 0.001$ and 4.16×10^{-5} , respectively, and 3 nmol at 1, 2 and 4 hrs, $P = 9.52 \times 10^{-11}$, 1.42×10^{-11} and 1.41×10^{-8} , respectively; IV $3 \mu\text{g kg}^{-1}$ at 1, 2 and 4 hrs, $P = 0.044$, 0.008 and 0.019 , respectively, and $10 \mu\text{g kg}^{-1}$ at 1, 2 and 4 hrs, $P = 1.37 \times 10^{-8}$, 6.81×10^{-14} and 3.23×10^{-4} , respectively. **b, c** $n = 6$ per treatment, except for 1 nmol BnOCPA, $n = 5$. **d** The analgesic effects of BnOCPA ($6 \mu\text{g kg}^{-1}$ IV) were prevented by the A_1 R antagonist DPCPX (1 mg kg^{-1} IP), but not the A_3 R-selective antagonist MRS1523 (2 mg kg^{-1} IP). Post hoc LSD comparisons across all four groups and four-time points (pre-dose, 1, 2 and 4 hrs; $F(15,116) = 26.8$, $P = 0$) revealed that BnOCPA at $6 \mu\text{g kg}^{-1}$ (IV) elicited significant analgesia compared to vehicle-treated animals at 1, 2, and 4 h post-dosing ($P = 4.69 \times 10^{-9}$, 3.50×10^{-9} , 4.69×10^{-9} , respectively), which persisted in the presence of the selective A_3 R antagonist MRS1523 over the same time period ($P = 4.42 \times 10^{-13}$, 3.38×10^{-14} , 1.81×10^{-10} , respectively). In contrast, the PWT in DPCPX-treated animals did not differ from those in the vehicle group ($P = 0.872$, 0.748 , 0.453 at 1, 2, and 4 h, respectively). $n = 11$ for BnOCPA and vehicle groups; $n = 6$ for the DPCPX group and $n = 5$ for the MRS1523 group. Averaged data are presented as mean \pm SEM. ns, not significant; *, $P < 0.05$; **, $P < 0.02$; ***, $P < 0.001$; ****, $P < 0.0001$. Source data are provided as a Source Data file.

maintained at 36.7°C via a thermocoupled heating pad (TCAT 2-LV; Physitemp). The trachea was cannulated and the femoral artery catheterised, and both were connected to pressure transducers (Digitimer) to record respiratory airflow and arterial blood pressure, respectively. Blood pressure and airflow signals were amplified using the NeuroLog system (Digitimer) connected to a micro1401 interface and acquired on a computer using Spike2 software (v7.08a; Cambridge Electronic Design). Arterial blood pressure recordings were used to derive heart rate (HR: $\text{beats}\cdot\text{minute}^{-1}$; BPM), and to calculate mean arterial blood pressure (MAP: $\text{Diastolic pressure} + 1/3[\text{Systolic Pressure} - \text{Diastolic pressure}]$). Airflow measurements were used to calculate: tidal volume (V_T ; mL; pressure sensors were calibrated with a 3 mL syringe), and respiratory frequency (f ; breaths min^{-1} ; BrPM). Minute ventilation (V_E ; mL min^{-1}) was calculated as $f \times V_T$.

Cardiovascular and respiratory parameters were allowed to stabilise before experiments began. A_1 R agonists were administered by intravenous (IV) injection and the changes in HR, MAP, f , V_T , and V_E were measured. In pilot studies, the optimal dose of adenosine was determined by increasing the dose until robust and reliable changes in HR and MAP were produced (1 mg kg^{-1}). The dose of CPA was adjusted until equivalent effects to adenosine were produced on HR and MAP ($6 \mu\text{g kg}^{-1}$). For BnOCPA we initially used $1 \mu\text{g kg}^{-1}$, but saw no agonist effect on HR and MAP. To ensure this was not a false negative we increased the dose of BnOCPA ($8 \mu\text{g kg}^{-1}$), which still gave no agonist effect on HR and MAP. However, as BnOCPA produced an antagonistic effect when co-administered with adenosine (Fig. 5, Supplementary Fig. 10b) and CPA (Fig. 6, Supplementary Fig. 11), it must have reached A_1 Rs at a high enough concentration to be physiologically active. These observations confirmed that the lack of agonistic effects on HR and MAP were not due to a type II error. $8 \mu\text{g kg}^{-1}$ BnOCPA was used for all further experiments. All injections were administered IV as a $350 \mu\text{l}\cdot\text{kg}^{-1}$ bolus.

In the experimental studies, rats either:

- received an injection of adenosine. After cardiorespiratory parameters returned to baseline (5–10 min), rats were given BnOCPA. After allowing sufficient time for any effect of BnOCPA to be observed, rats received adenosine with BnOCPA co-administered in a single injection. After cardiorespiratory parameters returned to baseline, rats were injected with CPA, or
- received an injection of CPA. After cardiorespiratory parameters returned to baseline (5–10 min) rats were given $8 \mu\text{g kg}^{-1}$ BnOCPA. After allowing sufficient time for any effect of BnOCPA to be observed, rats received CPA with $8 \mu\text{g kg}^{-1}$ BnOCPA co-administered in a single injection. After cardiorespiratory parameters returned to baseline, rats were injected with successive injections of $17 \mu\text{g kg}^{-1}$ and $25 \mu\text{g kg}^{-1}$ BnOCPA, with sufficient time given for any effect of BnOCPA to be observed.

To check that the volume of solution injected with each drug did not itself induce a baroreflex response leading to spurious changes in cardiorespiratory responses, equivalent volumes of saline (0.9%) were injected. These had no effect on either heart rate or MAP (Supplementary Fig. 10c). To confirm that repeated doses of adenosine produced the same response and that the responses did not run-down, rats were given two injections of adenosine (1 mg kg^{-1}). There was no significant difference in the changes in cardiovascular parameters produced by each adenosine injection (Supplementary Fig. 10d).

An additional series of experiments ($n = 4$) were undertaken to directly compare BnOCPA and CPA on respiration. Adult male Sprague–Dawley rats (400–500 g) were anaesthetised with urethane and instrumented as described above, with the exception that the arterial cannulation was not performed.

After allowing the animal to stabilise following surgery, BnOCPA ($8 \mu\text{g kg}^{-1}$) was administered. After a 20 min recovery period CPA ($6 \mu\text{g kg}^{-1}$) was administered. All injections were administered IV as a $350 \mu\text{l}\cdot\text{kg}^{-1}$ bolus. Changes in f , V_T , and V_E were measured. If the dosing occurred close to a respiratory event such as a sigh a second IV dose was administered, with 20 min recovery periods either side of the injection. Measurements for the effect of BnOCPA were time-matched to when CPA induced a change in respiration in the same preparation. As no difference was observed between the respiratory responses to BnOCPA in these rats ($n = 4$) and those instrumented for both cardiovascular and respiratory recordings ($n = 4$), the data were pooled ($n = 8$; Fig. 6a–d).

Spinal nerve ligation (Chung model⁹⁰). Adult male Sprague–Dawley rats, 7–8 weeks old, weighing around 250 g at the time of Chung model surgery, were purchased from Charles River UK Ltd. The animals were housed in groups of 4 in an air-conditioned room on a 12-hour light/dark cycle. Food and water were available *ad libitum*. They were allowed to acclimatise to the experimental environment for three days by leaving them on a raised metal mesh for at least 40 min. The baseline paw withdrawal threshold (PWT) was examined using a series of graduated von Frey hairs (see below) for 3 consecutive days before surgery and reassessed on the 6th to 8th day after surgery and on the 13th to 17th day after surgery before drug dosing.

Prior to surgery each rat was anaesthetised with 3% isoflurane mixed with oxygen (2 L min^{-1}) followed by an intramuscular injection of ketamine (60 mg kg^{-1}) plus xylazine (10 mg kg^{-1}). The back was shaved and sterilised with povidone-iodine. The animal was placed in a prone position and a para-medial incision was made on the skin covering the L4–6 level. The L5 spinal nerve was carefully isolated and tightly ligated with 6/0 silk suture. The wound was then closed in layers after a complete haemostasis. A single-dose of antibiotics (Amoxipen, 15 mg/rat , intraperitoneally, IP) was routinely given for prevention of infection after surgery. The animals were placed in a temperature-controlled recovery chamber until fully awake before being returned to their home cages. The vehicle (normal saline or DMSO) was administered via the IV route at $1 \text{ ml}\cdot\text{kg}^{-1}$ and via the intrathecal (IT) route at $10 \mu\text{l}$ for each injection. The A_1 R-selective antagonist DPCPX (1 mg kg^{-1}) and the A_3 R-selective antagonist MRS1523 (2 mg kg^{-1}) were delivered IP 30 mins before vehicle or BnOCPA treatment. The rats with validated neuropathic pain state were randomly divided into 11 groups: vehicle IV, BnOCPA at 1, 3, 6, $10 \mu\text{g kg}^{-1}$ IV; vehicle IT, BnOCPA at 0.3, 1, 3 nmol IT; $6 \mu\text{g kg}^{-1}$ BnOCPA IV plus 1 mg kg^{-1} DPCPX IP; $6 \mu\text{g kg}^{-1}$ BnOCPA IV plus 2 mg kg^{-1} MRS1523 IP groups and tested blind to treatment.

To test for mechanical allodynia the animals were placed in individual Perspex boxes on a raised metal mesh for at least 40 min before the test. Starting from the filament of lower force, each filament was applied perpendicularly to the centre of the ventral surface of the paw until slightly bent for 6 seconds. If the animal withdrew or lifted the paw upon stimulation, then a hair with force immediately lower than that tested was used. If no response was observed, then a hair with force immediately higher was tested. The highest value was set at 15 g. The lowest amount of force required to induce reliable responses (positive in 3 out of 5 trials) was recorded as the value of PWT. On the testing day, PWT were assessed before and 1, 2 and 4 h following BnOCPA or vehicle administration. The animals were returned to their home cages to rest (about 30 min) between two neighbouring testing time points. At the end of each experiment, the animals were deeply anaesthetised with isoflurane and killed by decapitation.

Rotarod test for motor function. A rotarod test was used to assess motor coordination following intravenous and intraperitoneal administration of BnOCPA. An accelerating rotarod (Ugo Basile) was set so speed increased from 6 to 80 rpm over 170 seconds. Male Sprague–Dawley rats ($n = 24$), 7 weeks of age (212–258 g) were trained on the rotarod twice daily for two days (≥ 2 trials per session) until performance times were stable. On the day of the experiment, three baseline trials were recorded. The compound was administered IP ($10 \mu\text{g kg}^{-1}$, $n = 6$) or IV via tail vein injection (10 and $25 \mu\text{g kg}^{-1}$, $n = 6$ per group). The control group received subcutaneous saline and the positive control group received subcutaneous morphine (15 mg kg^{-1}). Latency to fall (seconds) was measured in triplicate at 1, 2, 3 and 5 h post drug administration.

Constructs, transfections and generation of stable cell lines. Cell lines were maintained using standard subculturing routines as guided by the European Collection of Cell Culture (ECACC) and checked annually for mycoplasma infection using an EZ-PCR mycoplasma test kit from Biological Industries (Kibbutz Beit-Haemek, Israel). To investigate the signalling properties of the rat A_3R (rA_3R) and mutants of the human A_1R (hA_1R), stable cell lines were generated using Flp-In-CHO cells (ThermoFisher - R75807). Untagged hA_1R from sigNanoLuciferase (Nluc)- A_1R in pcDNA3.1+ and untagged rA_3R from sigNluc- A_3R in pcDNA3.1+ (both gifted by Dr Steve Briddon (University of Nottingham)) were cloned into the pcDNA5/FRT expression vector (Thermo Fisher Scientific). Mutations within the hA_1R were made using the QuikChange Lightning Site-Directed Mutagenesis Kit (Agilent Technologies) in accordance with the manufacturer's instructions. Constructs for generating Goa/b interfering and scrambled peptides were generated by PCR and cloned into the *Bam*HI/*Hind*III site of pcDNA3.1- as described in Gilchrist et al.⁶⁰. Prior to the initiator codon a Kozak sequence was included for enhanced translation. The peptide sequences used were: for Goa MGIANNLRGCGLY, for Gob MGIANKLRGCGLY, and for the scrambled peptide MGLNRGNAYLCIGMG was used. Constructs were sequenced to confirm fidelity. Flp-In-CHO cells were generated through co-transfection of the cell line with pcDNA5/FRT expression vector (Thermo Fisher Scientific) containing the WT or mutant hA_1R , or rA_3R , and the Flp recombinase expressing plasmid, pOG44 (Thermo Fisher Scientific), in accordance with the manufacturer's instructions. Co-transfection of cells in a T25 flask, with a total of $5 \mu\text{g}$ of adenosine receptor (AR)/pcDNA5/FRT and pOG44 (AR:pOG44 ratio of 1:9), was performed using Eugene HD (Promega), at a ratio of 3:1 (v/w) (Eugene:DNA). 24 h after transfection, cells were harvested and resuspended in growth media containing $600 \mu\text{g/ml}$ Hygromycin B (Thermo Fisher Scientific), and subsequently seeded into a fresh T25 flask. Media was replaced every 2–3 days and cells stably expressing the receptor of interest were selected using $600 \mu\text{g/ml}$ Hygromycin B. To generate CHO-K1 (European Collection of Authenticated Cell Cultures (ECAC) catalogue number 85051005) cells stably expressing the rat $A_{2A}R$ (CHO-K1- $rA_{2A}R$), CHO-K1 cells were seeded onto a 6-well plate and transfected with $1 \mu\text{g}$ $rA_{2A}R$ using Eugene HD (Promega) at a ratio of 3:1 (v/w) (Eugene:DNA). 48 h after transfection, media was replaced with growth media containing $800 \mu\text{g/ml}$ G418 (Thermo Fisher Scientific) and changed every 2–3 days until cells were $>80\%$ confluent. To investigate rat A_1R -mediated signalling, CHO-K1 cells seeded onto a 6-well plate were transiently transfected with $1 \mu\text{g}$ rat A_1R (rA_1R) using Eugene HD (Promega) at a ratio of 3:1 (v/w) (Eugene:DNA), for 48 h. The plasmids encoding the rA_1R and $rA_{2A}R$ (Nluc- A_1R /pcDNA3.1(+) and Nluc- $A_{2A}R$ /pcDNA3.1(+), respectively) were kindly gifted by Stephen Hill and Stephen Briddon (University of Nottingham).

Cell signalling assays. CHO cell lines expressing ARs of interest (including mutants of the hA_1R) were routinely cultured in Ham's F-12 nutrient mix supplemented with 10% foetal bovine serum (FBS), at 37°C with 5% CO_2 , in a humidified atmosphere. For cAMP accumulation experiments, cells were seeded at a density of 2000 cells per well of a white 384-well optiplate and stimulated, for 30 min, with a range of agonist concentrations ($100 \text{ pM} - 100 \mu\text{M}$) in the presence of $25 \mu\text{M}$ rolipram (Cayman Chemicals). For cAMP inhibition experiments, cells were co-stimulated with $1 \mu\text{M}$ forskolin and a range of agonist concentrations ($1 \text{ pM} - 100 \mu\text{M}$), in the presence or absence of $1 \mu\text{M}$ antagonist. cAMP levels were then determined using a LANCE® cAMP kit as described previously^{33,111}.

For determination of individual Gai/o/z couplings, CHO-K1- hA_1R cells (made in-house) were transfected with pcDNA3.1-GNAZ or, pcDNA3.1 containing pertussis toxin (PTX) insensitive Gai/o protein mutants (C351I, C352I, C351I, C351I, C351I, for Gi1, Gi2, Gi3, Goa, Gob, respectively, obtained from cDNA Resource Centre; www.cdna.org), using 500 ng plasmid and Eugene HD at a 3:1 (v/w) (Eugene:Plasmid) ratio. Cells were then incubated for 24 h before addition of 100 ng/ml PTX, to inhibit activity of endogenous Gai/o, and then incubated for a further 16–18 h. Transfected cells were then assayed as per cAMP inhibition experiments, but co-stimulated with agonist and 100 nM forskolin.

β -arrestin recruitment assays. HEK 293 T cells (ATCC CRL-3216) were routinely grown in DMEM/F-12 GlutaMAX™ (Thermo Fisher Scientific) supplemented with 10% foetal bovine serum (FBS; F9665, Sigma-Aldrich) and 1x antibiotic-antimycotic solution (DMEM complete; Thermo Fisher Scientific). For analysis of β -arrestin recruitment following ligand stimulation at the hA_1R or hA_3R , HEK 293 T cells in a single well of 6-well plate (confluency $\geq 80\%$) were

transiently co-transfected with either A_1R -Nluc or A_3R -Nluc, β -arrestin1/2-YFP and hGRK1-6, or pcDNA3.1 vector (total $2 \mu\text{g}$, at a AR: β -arrestin:hGRK ratio of 1:5:4) using polyethylenimine (PEI, 1 mg/ml , MW = $25,000 \text{ g/mol}$; Polysciences Inc) at a DNA:PEI ratio of 1:6 (w/w). As a negative control for the A_1R , transfections were also set up in the absence of β -arrestin1/2-YFP. Briefly, in sterile tubes containing 150 mM NaCl, DNA or PEI was added (final volume $50 \mu\text{l}$) and allowed to incubate at room temperature for 5 min before mixing together and incubating for a further 10 min prior to adding the combined mix dropwise to the cells. 24 h post-transfection, HEK 293 T cell were harvested, resuspended in reduced serum media (MEM, NEAA; Thermo Fisher Scientific) supplemented with 1% L-glutamine (2 mM final; Thermo Fisher Scientific), 2% FBS and 1x antibiotic-antimycotic solution and seeded ($50,000$ cells/well) in a poly-L-lysine-coated (MW: $150,000 - 300,000 \text{ Da}$; Sigma-Aldrich) white 96-well plate (PerkinElmer Life Sciences). 24 h post seeding, media was removed, cells gently washed in PBS and $90 \mu\text{l}$ of furimazine ($4 \mu\text{M}$)-containing solution added (PBS supplemented with 0.49 mM MgCl_2 , 0.9 mM CaCl_2 and 0.1% BSA) to each well before incubating in the dark for 10 min. After incubation, $10 \mu\text{l}$ of agonist (NECA, CPA, adenosine, BnOCPA) was added ($0.01 \mu\text{M}$ to $10 \mu\text{M}$) and filtered light emissions measured at 450 nm and 530 nm every minute for 1 h using a Mithras LB 940 (Berthold technology) using MikroWin 2000 software. Here, Nluc on the C-terminus of A_1R or A_3R acted as the BRET donor (luciferase oxidising its substrate) and YFP acted as the fluorescent acceptor. Vehicle control (1% DMSO) was added to determine background emission, and data was corrected for baseline reading, vehicle and the response obtained in the absence of YFP- β -arrestin1/2, when appropriate.

Radioligand binding. Radioligand displacement assays were conducted using crude membrane preparations ($100 \mu\text{g}$ protein per tube) acquired from homogenisation of CHO-K1- hA_1R cells in ice-cold buffer (2 mM MgCl_2 , 20 mM HEPES, pH 7.4). The ability to displace binding of the A_1R -selective antagonist radioligand, 1,3- ^3H -dipropyl-8-cyclopentylxanthine (^3H -DPCPX) at a concentration (1 nM) around the K_d value (1.23 nM , as determined by saturation binding experiments) by increasing concentrations of NECA, adenosine, CPA, BnOCPA or HOCPA ($0.1 \text{ nM} - 10 \mu\text{M}$) allowed the binding affinities (K_i) to be determined. Non-specific binding was determined in the presence of $10 \mu\text{M}$ DPCPX. Membrane incubations were conducted in Sterilin™ scintillation vials (Thermo Fisher Scientific; Wilmington, Massachusetts, USA) for 60 min at room temperature. Free radioligand was separated from bound radioligand by filtration through Whatman® glass microfibre GF/B 25 mm filters (Sigma-Aldrich). Each filter was then placed in a Sterilin™ scintillation vial and radioactivity determined by: addition of 4 mL of Ultima Gold XR liquid scintillant (PerkinElmer), overnight incubation at room temperature and the retained radioactivity determined using a Beckman Coulter LS 6500 Multi-purpose scintillation counter (Beckman Coulter Inc.; Indiana, USA).

NanoBRET ligand-binding studies. Real-time pharmacological interactions between ligands and receptors was quantitated using NanoBRET as described previously¹¹². In brief, using N-terminally Nluc-tagged rA_1R , $rA_{2A}R$ or rA_3R -expressing HEK 293 cell lines, competition binding assays were conducted. In all antagonist assays CA200645, which acts as a fluorescent antagonist with a slow off-rate¹¹³, was used, with the exception of the rat A_3R where the fluorescent compound was AV039¹¹⁴. The data was fitted with the 'one-site - K_i model' derived from the Cheng and Prusoff equation, built into Prism to determine affinity (pK_i) values for all unlabelled agonists at all AR subtypes assayed. For the hA_1R , we also performed an agonist binding competition assay using NECA-TAMRA (Noel et al., unpublished). Here data was fitted with the 'two-site K_i model', built into Prism to determine high affinity and low affinity values for the unlabelled agonists. For all ARs, filtered light emission at 450 nm and $>610 \text{ nm}$ ($640 - 685 \text{ nm}$ band pass filter) was measured using a Mithras LB 940 and the raw BRET ratio calculated by dividing the 610 nm emission with the 450 nm emission. The Nluc acts as the BRET donor (luciferase oxidising its substrate) and CA200645/AV039/NECA-TAMRA acted as the fluorescent acceptor. CA200645 was used at 25 nM , as previously reported¹¹⁵, AV039 was used at 100 nM ¹¹² and NECA-TAMRA at its K_d of $15.2 \mu\text{M}$ (Noel et al., unpublished). BRET was measured following the addition of the Nluc substrate, Furimazine ($0.1 \mu\text{M}$). Non-specific binding was determined using a high concentration of unlabelled antagonist, DPCPX for rA_1R , ZM241385 for the $rA_{2A}R$ and MRS1220 for rA_3R .

TRUPATH G protein dissociation assay. Cells were plated in a density of $1,500,000$ cells/well in a 6-well plate and grown in DMEM /F-12 GlutaMAX™ media (Thermo Fisher Scientific, UK) supplemented with 10% FBS (Sigma, UK) and 1% AA (Sigma, UK). After being grown overnight, cells in each well were transfected using polyethylenimine 25 kDa (PEI, Polysciences Inc., Germany) at a 6:1 ratio of PEI to DNA, diluted in 150 mM NaCl. Cells were transfected with hA_1R , Goa-RLuc8 or Gob-RLuc8, $\text{G}\beta_3$, $\text{G}\gamma_8$ -GFP2, and pcDNA3.1 with the ratio of 1:1:1:1 (400 ng per construct) in accordance with previously published methods⁵⁵. Go (either Goa-RLuc8, or Gob-RLuc8), $\text{G}\beta_3$ and $\text{G}\gamma_8$ -GFP2 constructs were purchased as part of the TRUPATH sensor kit from Addgene, pcDNA3.1- A_1R was obtained from cDNA resource centre, and pcDNA3.1 (-) zeo was purchased from Invitrogen. After 24 h, cells were trypsinised and re-seeded onto poly-L-lysine (PLL)-coated white 96-well plates (Greiner, UK) at the density of $50,000$ cells/well in a complete DMEM/F-12 medium. After grown overnight, the culture

media was discarded and replaced with 80 μ l assay buffer (1 \times Hank's balanced salt solution (HBSS) with calcium, supplemented with 20 mM HEPES and 0.1% BSA at pH 7.4). The assay was started by adding 10 μ l of coelenterazine 400a (Nanolight technology, USA) to a final concentration of 5 μ M. The plates were then incubated in the dark for 5 min, prior to the addition of 10 μ l compounds (in a range of 0.01 nM – 1 μ M). In order to investigate the effect of interfering peptides on Goa and Gob activation, cells were transfected with the TRUPATH constructs for Goa and Gob with the A₁R as described above. However, the vector was replaced by either interfering or scrambled peptides, as appropriate, with increasing concentration: 0, 100, and 400 ng and was complemented by pcDNA3.1(-) up to 400 ng. CPA 10 μ l was used as the ligand in a range of 1 nM–1 μ M. BRET signal was recorded for 30 min on a Mithras LB940 plate reader allowing sequential integration of signal detected from GFP2 (515 nm) over Rluc8 (400 nm). Net BRET ratio was used to generate the concentration-response curve by taking 11-minute time-point after baseline correction. Data was analysed as change in the presence of the interfering peptides relative to control alone at 1 μ M CPA.

Statistics and reproducibility

Data and statistical analysis. Concentration-response curves for the effects of A₁R agonists on synaptic transmission were constructed in OriginPro 2018 (OriginLab; Northampton, MA, USA) and fitted with a logistic curve using the Levenberg Marquadt iteration algorithm. OriginPro 2018 was also used for statistical analysis. Statistical significance was tested as indicated in the text using paired or unpaired two-tailed t-tests or one-way or two-way ANOVAs with repeated measures (RM) as appropriate. Bonferroni corrections for multiple comparisons were performed. All in vitro cell signalling assay data was analysed using Prism 8.4 (Graphpad software, San Diego, CA), with all concentration-response curves being fitted using a 3 parameter logistic equation to calculate response range and IC₅₀. All cAMP data was normalised to a forskolin concentration-response curve ran in parallel to each assay. Where appropriate the operational model of receptor agonism^{52,111} was used to obtain efficacy (log τ) and equilibrium dissociation constant (log K_A) values. Calculation of bias factors ($\Delta\log(\text{Tau}/K_A)$) relative to adenosine was performed as described in Weston et al. (2016)¹¹¹. Error for this composite measure was propagated by applying the following Eq. (1).

$$\text{Pooled SEM} = \sqrt{(\text{SEM}_A)^2 + (\text{SEM}_B)^2} \quad (1)$$

Where, σ_A and σ_B are the standard deviations of measurement A and B with mean of \bar{x}_A and \bar{x}_B is the composite mean and n is the number of repeats.

Single-dose Schild analysis was performed on data using BnOCPA as an antagonist to adenosine in the cAMP assays so enabling determination of BnOCPA's affinity constant (K_A) using the following Eq. (2)

$$\frac{D'}{D} = 1 + [A]K_2 \quad (2)$$

where D' and $D = \text{EC}_{50}$ values of adenosine with and without BnOCPA present, respectively, $[A]$ = the concentration of BnOCPA, and K_2 = the affinity constant (K_A) of the BnOCPA⁵⁸.

Statistical significance relative to adenosine was calculated using a one-way ANOVA with a Dunnett's post-test for multiple comparisons. Radioligand displacement curves were fitted to the one-site competition binding equation yielding log(Ki) values. One-way ANOVA (Dunnett's post-test) was used to determine significance by comparing the log(Ki) value for each compound when compared to adenosine. To determine the extent of ligand-induced recruitment of β -arrestin2-YFP to either the A₁R or A₃R, the BRET signal was calculated by subtracting the 530 nm/450 nm emission for vehicle-treated cells from ligand-treated cells (ligand-induced Δ BRET). Δ BRET for each concentration at 5 min (maximum response) was used to produce concentration-response curves.

All in vivo cardiovascular and respiratory data were analysed using OriginPro 2018. One-way ANOVAs, with repeated measures as appropriate, and with Bonferroni correction for multiple comparisons were used. Statistical significance for the effects of IV saline and the antagonist effect of BnOCPA on CPA were tested using two-tailed paired t-tests. Data are reported throughout as mean \pm SEM and n values are reported for each experiment. For the neuropathic pain studies, one-way ANOVAs with Fisher's Least Significant Difference (LSD) post hoc test was used to compare drug treatment groups to the vehicle group (OriginPro 2018). The significance level was set at $P < 0.05$, with actual P values reported in the figure legends and summaries, by way of abbreviations and asterisks, on the graphs: ns, not significant; * $P < 0.05$; ** $P < 0.02$; *** $P < 0.001$; **** $P < 0.0001$.

Reproducibility. Samples sizes for in vitro pharmacological or in vivo cardiorespiratory experiments were based on prior experience and were routinely in excess of 4 individual biological replicates. In many instances the pool of replicates was added to over time via interleaved experiments with other compounds and often by other investigators, ensuring the consistency and reproducibility of experimental observations. Data was only excluded when technical failures occurred. Randomisation and blinding was not performed for in vitro or cardiorespiratory studies. In the pain and rotarod studies, the sample sizes for which (typically 6 animals) were based on prior experience, the experimenters were blinded to the reagents used. For the pain studies, all animals were pre-screened for hypersensitivity (von

Frey hair) when they arrived, and those that showed this, i.e., a paw withdrawal threshold (PWT) less than 8 g, were eliminated from the study. Those rats successfully developing mechanical allodynia (with PWT lower than 4 g) were randomly assigned into different groups according to their PWT values of pre-surgery, 1 week post-surgery and pre-dosing to ensure a balanced distribution across groups. For the rotarod studies, rats were randomly assigned to treatment groups by animal care technicians not involved in the experimental studies. Experiments occurred over a period of time with various types of manipulations interleaved to avoid batch effects. Key observations were replicated with different batches of animals and reagents and by different experimenters. Results across different independent labs working in different experimental systems were consistent with the main themes and conclusions of the study.

Drugs and substances. Drugs were made up as stock solutions (1–10 mM) and then diluted in aCSF or saline on the day of use. BnOCPA³⁴ ((2R,3R,4S,5R)–2-(6-((1R,2R)–2-benzyloxycyclopentyl)amino)–9H-purin-9-yl)–5-(hydroxymethyl)oxolane-3,4-diol) and HOCPA⁴⁷ ((2R,3R,4S,5R)–2-(6-((1R,2R)–2-hydroxycyclopentyl)amino)–9H-purin-9-yl)–5-(hydroxymethyl)oxolane-3,4-diol), the [(1R,2R)–2-hydroxycyclopentyl]amino bis-epimer of known A₁R agonist GR79236⁴⁹, were synthesised as described previously³³ and dissolved in dimethyl-sulphoxide (DMSO, 0.01% final concentration). Adenosine, 8-CPT (8-cyclopentyltheophylline), NECA (5'-(N-Ethylcarboxamido) adenosine), DPCPX, ZM241385, MRS1220 and CPA (N⁶-Cyclopentyladenosine) were purchased from Sigma-Aldrich (Poole, Dorset, UK). MRS1523 was purchased from Cayman Chemicals (Cambridge Bioscience Ltd., Cambridge UK). [³H]-DPCPX was purchased from PerkinElmer (Life and Analytical Sciences, Waltham, MA). CA200645 and peptides for interfering with G protein signalling were obtained from Hello Bio (Bristol, UK) and were based on published sequences⁶⁰. NECA-TAMARA was synthesised in-house (Noel et al., in preparation), while AV039, a highly potent and selective fluorescent antagonist of the human A₃R based on the 1,2,4-Triazolo[4,3-a]quinoxalin-1-one linked to BY630 was kindly gifted to us by Stephen Hill and Stephen Briddon (University of Nottingham). For G_{oa} the peptide had a sequence of MGIANNLRGCGLY. The scrambled version was LNRGNAYLCIGMG. For G_{ob} the peptide had a sequence of MGIAKNLRGCGLY. Peptides were made up as stock solutions (2 mM) and stored at –20 °C. The stock solutions were dissolved in filtered intracellular solution just before use.

BnOCPA Pharmacokinetics. The stability in solution and metabolism of BnOCPA (0.1 μ M or 1 μ M) was assessed by Eurofins Panlabs (Supplementary Data 1). The parameters examined were: half-life ($t_{1/2}$) in PBS (1 μ M BnOCPA, 37 °C, pH 7.4; Assay #600); $t_{1/2}$ in human plasma (1 μ M BnOCPA, 37 °C; Assay #887) and intrinsic clearance by human liver microsomes (0.1 μ M BnOCPA, 0.1 mg/ml, 37 °C; Assay #607).

Half-life determination in PBS. At the end of the incubation at each of the time points (0, 1, 2, 3, 4 h), an equal volume of an organic mixture (acetonitrile/methanol, 50/50 v/v) was added to the incubation mixture. Samples were analysed by HPLC-MS/MS and corresponding peak areas were recorded for each analyte. The ratio of precursor compound remaining after each time-point relative to the amount present at time 0, expressed as a percentage, is reported as chemical stability. The $t_{1/2}$ was estimated from the slope of the initial linear range of the logarithmic curve of compound remaining (%) versus time, assuming first-order kinetics.

Half-life determination in human plasma. At the end of incubation at each of the time points (0, 0.5, 1, 1.5, 2 h), acetonitrile was added to the incubation mixture followed by centrifugation. Samples were analysed by HPLC-MS/MS and peak areas were recorded for each analyte. The area of precursor compound remaining after each of the time points relative to the amount remaining at time 0, expressed as a percentage, was calculated. Subsequently, the $t_{1/2}$ is estimated from the slope of the initial linear range of the logarithmic curve of compound remaining (%) versus time, assuming first-order kinetics.

Intrinsic clearance by human liver microsomes. Metabolic stability, expressed as a percentage of the parent compound remaining, was calculated by comparing the peak area of the compound at the time-point (0, 15, 30, 45, 60 min) relative to that at time 0. The $t_{1/2}$ was estimated from the slope of the initial linear range of the logarithmic curve of compound remaining (%) vs. time, assuming the first-order kinetics. The apparent intrinsic clearance (CL_{int} , in μ L/min/mg) was calculated according to the following Eq. (3):

$$CL_{int} = \frac{0.693}{t_{1/2} \times (0.0001 \text{ mg protein}/\mu\text{L})} \quad (3)$$

The behaviour of BnOCPA was compared to appropriate standards. Data is available in Supplemental Data File 1

Molecular dynamics simulations

Ligand parameterisation. The CHARMM36^{116,117}/CGenFF^{118–120} force field combination was employed in all the MD simulations performed. Initial topology and parameter files of BnOCPA, HOCPA, and PSB36 were obtained from the

Table 1 Summary of the simulations performed.

Ligand	MD approach	# Replicas	Total simulated time*
BnOCPA	SuMD	6	1.9 μ s
BnOCPA	SuMD-Metadynamics	5	4.3 μ s
HOCPA	SuMD	5	3.4 μ s
BnOCPA (bound state after dynamic docking)	Metadynamics	3	0.75 μ s
BnOCPA(A)	Classic MD	6	9.0 μ s
BnOCPA(B)	Classic MD	6	9.0 μ s
BnOCPA(C)	Classic MD	3	3.0 μ s
BnOCPA(D)	Classic MD	6	9.0 μ s
HOCPA	Classic MD	4	8.0 μ s
PSB36	Classic MD	4	6.0 μ s
Apo A ₁	Classic MD	4	8.0 μ s
G α CT Goa (BnOCPA)	SuMD + Classic MD	10	0.36 μ s + 3.0 μ s
G α CT Gob (BnOCPA)	SuMD + Classic MD	10	0.33 μ s + 3.0 μ s
G α CT Gi2 (BnOCPA)	SuMD + Classic MD	10	0.37 μ s + 3.0 μ s
G α CT Gob (HOCPA)	SuMD + Classic MD	10	0.29 μ s + 3.0 μ s
BnOCPA(D):Gob	Classic MD	4	4.0 μ s
BnOCPA(B):Gob	Classic MD	3	3.0 μ s
HOCPA:Gob	Classic MD	4	4.0 μ s
BnOCPA(D):Goa	Classic MD	5	5.0 μ s
BnOCPA(B):Goa	Classic MD	4	4.0 μ s

*For SuMD and SuMD-metadynamics simulations the time is the sum of productive SuMD time windows. (A), (B), (C) and (D) indicate the respective BnOCPA binding modes.

Paramchem webserver¹¹⁸. Higher penalties were associated with a few BnOCPA dihedral terms, which were therefore optimised at the HF/6-31 G* level of theory using both the high throughput molecular dynamics (HTMD)¹²¹ parameterise functionality and the visual molecular dynamics (VMD)¹²² Force Field Toolkit (ffTK)¹²³, after fragmentation of the molecule. Short MD simulations of BnOCPA in water were performed to visually inspect the behaviour of the optimised rotatable bonds.

Systems preparation for fully dynamic docking of BnOCPA and HOCPA. Coordinates of the A₁R in the active, adenosine- and G protein-bound state were retrieved from the Protein Data Bank^{124,125} database (PDB ID 6D9H⁷⁷). Intracellular loop 3 (ICL3) which is missing from PDB ID 6D9H was rebuilt using Modeller 9.19^{126,127}. The G protein, with the exception of the C-terminal helix (helix 5) of the G protein alpha subunit (the key region responsible for the receptor TM6 active-like conformation) was removed from the system as in previous work^{128,129}. BnOCPA and HOCPA were placed in the extracellular bulk, in two different systems, at least 20 Å from the receptor vestibule. The resulting systems were prepared for simulations using in-house scripts able to exploit both python HTMD¹²¹ and Tool Command Language (TCL) scripts. Briefly, this multi-step procedure performs the preliminary hydrogen atoms addition by means of the pdb2pqr¹³⁰ and propka3¹³¹ software, considering a simulated pH of 7.0 (the proposed protonation of titratable side chains was checked by visual inspection). Receptors were then embedded in a square 80 Å × 80 Å 1-palmitoyl-2-oleyl-sn-glycerol-3-phosphocholine (POPC) bilayer (previously built by using the VMD Membrane Builder plugin 1.1, Membrane Plugin, Version 1.1; <http://www.ks.uiuc.edu/Research/vmd/plugins/membrane/>) through an insertion method¹³², considering the A₁R coordinates retrieved from the OPM database¹³³ to gain the correct orientation within the membrane. Lipids overlapping the receptor transmembrane bundle were removed and TIP3P water molecules¹³⁴ were added to the simulation box (final dimensions 80 Å × 80 Å × 125 Å) using the VMD Solvate plugin 1.5 (Solvate Plugin, Version 1.5; <http://www.ks.uiuc.edu/Research/vmd/plugins/solvate/>). Finally, overall charge neutrality was achieved by adding Na⁺/Cl⁻ counter ions (concentration of 0.150 M) using the VMD Autoionize plugin 1.3 (Autoionize Plugin, Version 1.3; <http://www.ks.uiuc.edu/Research/vmd/plugins/autoionize/>). All histidine side chains were considered in the delta tautomeric state, with the exception of H251 (epsilon tautomer) and H278 (protonated).

The MD engine ACEMD¹³⁵ was employed for both the equilibration and productive simulations. Systems were equilibrated in isothermal-isobaric conditions (NPT) using the Berendsen barostat¹³⁶ (target pressure 1 atm), the Langevin thermostat¹³⁷ (target temperature 300 K) with a low damping factor of 1 ps⁻¹ and with an integration time step of 2 fs. Clashes between protein and lipid atoms were reduced through 2000 conjugate-gradient minimisation steps before a 2 ns long MD simulation was run with a positional constraint of 1 kcal mol⁻¹ Å⁻² on protein and lipid phosphorus atoms. Twenty nanoseconds of MD simulation were then performed constraining only the protein atoms. Lastly, positional constraints were applied only to the protein backbone alpha carbons for a further 5 ns.

Dynamic docking of BnOCPA and HOCPA. The supervised MD (SuMD) approach is an adaptive sampling method¹³⁸ for simulating binding events in a timescale one or two

orders of magnitudes faster than the corresponding classical (unsupervised) MD simulations¹³⁹. SuMD has been successfully applied to small molecules and peptides^{140–146}. In the present work, the distances between the centres of mass of the adenine scaffold of the A₁R agonist and N254^{6,55}, F171^{ECL2}, T277^{7,42} and H278^{7,43} of the receptor were considered for the supervision during the MD simulations. The dynamic docking of BnOCPA was hindered by the ionic bridge formed between the E172^{ECL2} and K265^{ECL3} side chains. A metadynamics^{147–149} energetic bias was therefore introduced in order to facilitate the rupture of this ionic interaction, thus favoring the formation of a bound complex. More precisely, Gaussian terms (height = 0.01 kcal mol⁻¹ and widths = 0.1 Å) were deposited every 1 ps along the distance between the E172^{ECL2} carboxyl carbon and the positively charged K265^{ECL3} nitrogen atom using PLUMED 2.3¹⁵⁰. A similar SuMD-metadynamics hybrid approach was previously employed to study binding/unbinding kinetics¹⁵¹ on the A_{2A}R subtype. For each replica (Table 1), when the ligands reached a bound pose (i.e. a distance between the adenine and the receptor residues centres of mass <3 Å), a classic (unsupervised and without energetic bias) MD simulation was performed for at least a further 100 ns.

BnOCPA bound state metadynamics. We decided to perform a detailed analysis of the role played by the E172^{ECL2}-K265^{ECL3} ionic interaction in the dynamic docking of BnOCPA. Three 250 ns long well-tempered¹⁵² metadynamics simulations were performed using the bound state obtained from a previous dynamic docking simulation, which resulted in binding mode A, as a starting point. The collective variables (CVs) considered were: i) the distance between the E172^{ECL2} carboxyl carbon and the positively charged K265^{ECL3} nitrogen atom and ii) the dihedral angle formed by the 4 atoms linking the cyclopentyl ring to the phenyl moiety (which was the most flexible ligand torsion during the previous SuMD simulations). Gaussian widths were set at 0.1 Å and 0.01 radians respectively, heights at 0.01 kcal/mol⁻¹, and the deposition was performed every 1 ps (bias-factor = 5). Although complete convergence was probably not reached, three replicas (Table 1) allowed sampling of three main energetic minima on the energy surface (Supplementary Fig. 8); these correspond to the representative binding poses shown in Fig. 3d to f.

Classic MD simulations of BnOCPA binding modes A, B, C and D. To test the hypothesis that BnOCPA and HOCPA may differently affect TM6 and/or TM7 mobility when bound to A₁R (and to further sample the stability of each BnOCPA binding mode), putative binding conformations A, B and C (Fig. 3) were superposed to the experimental A₁R active state coordinates with the modelled ICL3. This should have removed any A₁R structural artefacts, possibly introduced by metadynamics. As reference and control, two further systems were considered: i) the pseudo-apo A₁R and ii) the selective A₁R antagonist PSB36⁷² superposed in the same receptor active conformation (Table 1). The BnOCPA binding mode D was modelled from mode B by rotating the dihedral angle connecting the cyclopentyl ring and the N6 nitrogen atom in order to point the benzyl of the agonist toward the hydrophobic pocket underneath ECL3 (Fig. 3g) delimited by L253^{6,56}, T257^{6,52}, K265^{ECL3}, T270^{7,35}, and L269^{7,34}. The G protein atoms were removed, and the resulting systems prepared for MD as reported above. A similar comparison was performed in a milestone study on the β_2 adrenergic receptor⁷⁶ which sought to describe the putative deactivation mechanism of the receptor.

Dynamic docking of the Goa, Gob and Gi2-GaCT helix. A randomly extracted frame from the classic MD performed on the BnOCPA:A₁R complex was prepared for three sets of simulations placing the GaCT helix 5 (last 27 residues) of the Ga proteins Goa, Gob and Gi2 in the intracellular solvent bulk side of the simulation boxes. As a further control, a frame from the classic MD performed on the unbiased ligand HOCPA:A₁R complex was randomly extracted and prepared along with the Gob-GaCT. The resulting four systems were embedded in a POPC membrane and prepared as reported above.

The different structural effects putatively triggered by BnOCPA and HOCPA on the recognition mechanism of Goa, Gob and Gi2-GaCT were studied by performing 10 SuMD replicas (Table 1). During each replica (Video S3), the distance between the centroid of the GaCT residues 348-352 and the centroid of the A₁R residues D42^{2,37}, I232^{6,33}, and Q293^{8,48} was supervised until it reached a value lower than 8 Å. A classic MD simulation was then run for a further 300 ns.

Classic MD simulations on the A₁R:Goa and Gob complexes. The A₁R cryo-EM structure (PDB ID 6D9H) was used as template for all the five systems simulated (Table 1). The endogenous agonist adenosine was removed and HOCPA and BnOCPA (modes B and D) were inserted in the orthosteric site superimposing 6D9H to the systems prepared for the classic MD simulations in the absence of G protein. ICL3 was not modelled, nor were the missing part of the G protein α subunit. As subunits β and γ were removed, the Ga NT helix was truncated to residue 27 to avoid unnatural movements (NT is constrained by G β in 6D9H). The Ga subunit was mutated according to the Goa and Gob primary sequences⁸⁷ using in-house scripts. The resulting five systems (Table 1) were embedded in a POPC membrane and prepared as reported above.

Analysis of the classic MD simulations. During the classic MD simulations that started from Modes A-C (Fig. 3d-g), BnOCPA had the tendency to explore the three conformations by rapidly interchanging between the three binding modes. In order to determine the effect exerted on the TM domain by each conformation, 30 μ s of MD simulations (Table 1: BnOCPA mode A, BnOCPA mode B, BnOCPA mode C, BnOCPA mode D) were subjected to a geometric clustering. More precisely, a simulation frame was considered in pose A if the distance between the phenyl ring of BnOCPA and the I175^{ECL2} alpha carbon was less than 5 Å; in pose B if the distance between the phenyl ring of BnOCPA and the L258^{6,59} alpha carbon was less than 6 Å, and in pose C if the distance between the phenyl ring of BnOCPA and the Y271^{7,36} alpha carbon was less than 6 Å. During the MD simulations started from mode D (Fig. 3g), a frame was still considered in mode D if the root mean square deviation (RMSD) of the benzyl ring to the starting equilibrated conformation was less than 3 Å. For each of the resulting four clusters, the RMSD of the GPCR conserved motif NPXXY (N^{7,49} PIV Y^{7,53} in the A₁R; Supplementary Fig. 9) was computed using Plumed 2.3¹⁵⁰ considering the inactive receptor state as reference, plotting the obtained values as frequency distributions (Fig. 3i, j). Rearrangement of the NPXXY motif, which is located at the intracellular half of TM7, is considered one of the structural hallmarks of GPCR activation⁷⁹. Upon G protein binding, it moves towards the centre of the receptor TM bundle (Supplementary Fig. 9). Unlike other activation micro-switches (e.g. the break/formation of the salt bridge between R^{3,50} and E^{6,30}), this conformational transition is believed to occur in timescales accessible to MD simulations⁷⁶.

Hydrogen bonds and atomic contacts were computed using the GetContacts analysis tool (<https://github.com/getcontacts/getcontacts>) and expressed in terms of occupancy (the percentage of MD frames in which the interaction occurred).

Analysis of the Goa, Gob and Gi2-GaCT classic MD simulations after SuMD. For each system, only the classic MD simulations performed after the GaCT reached the A₁R intracellular binding site were considered for the analysis.

The RMSD values to the last 15 residues of the Gi2-GaCT reported in the A₁R cryo-EM PDB structure 6D9H were computed using VMD¹²². The MD frames associated with the peaks in the RMSD plots (states CS1, MS1, MS2 and MS3 in Fig. 4a, d) were clustered employing the VMD Clustering plugin (<https://github.com/luisico/clustering>) by selecting the whole GaCT helixes alpha carbon atoms and a cutoff of 3 Å.

Reporting summary. Further information on research design is available in the Nature Research Reporting Summary linked to this article.

Data availability

The active cryo-EM structure of the A₁R (PDB code 6D9H) was retrieved from <https://www.rcsb.org/structure/6d9h>; the human neurotensin receptor 1 (PDB code 6OSA) from <https://www.rcsb.org/structure/6OSA>, and the β 2 adrenergic receptor (PDB code 6E67) from <https://www.rcsb.org/3d-view/6e67>. Source data are provided with this paper.

Code availability

SuMD scripts used for this manuscript, and newer versions, are provided as Supplemental Data File 2. AceMD software is available from Acellera's website www.acellera.com.

Received: 21 July 2020; Accepted: 23 June 2022;

Published online: 18 July 2022

References

- Hauser, A. S., Attwood, M. M., Rask-Andersen, M., Schiöth, H. B. & Gloriam, D. E. Trends in GPCR drug discovery: new agents, targets and indications. *Nat. Rev. Drug Discov.* **16**, 829 (2017).
- Congreve, M., de Graaf, C., Swain, N. A. & Tate, C. G. Impact of GPCR structures on drug discovery. *Cell* **181**, 81–91 (2020).
- Kenakin, T. Is the quest for signaling bias worth the effort? *Mol. Pharm.* **93**, 266–269 (2018).
- Michel, M. C. & Charlton, S. J. Biased agonism in drug discovery—is it too soon to choose a path? *Mol. Pharm.* **93**, 259–265 (2018).
- Jacobson, K. A. & Muller, C. E. Medicinal chemistry of adenosine, P2Y and P2X receptors. *Neuropharmacology* **104**, 31–49 (2016).
- Borea, P. A., Gessi, S., Merighi, S., Vincenzi, F. & Varani, K. Pharmacology of adenosine receptors: the state of the art. *Physiol. Rev.* **98**, 1591–1625 (2018).
- Sawynok, J. Adenosine receptor targets for pain. *Neuroscience* **338**, 1–18 (2016).
- Headrick, J. P., Ashton, K. J., Rosemeyer, R. B. & Peart, J. N. Cardiovascular adenosine receptors: expression, actions and interactions. *Pharm. Ther.* **140**, 92–111 (2013).
- Dunwiddie, T. V. & Masino, S. A. The role and regulation of adenosine in the central nervous system. *Annu Rev. Neurosci.* **24**, 31–55 (2001).
- Vecchio, E. A. et al. New paradigms in adenosine receptor pharmacology: allostery, oligomerization and biased agonism. *Br. J. Pharm.* **175**, 4036–4046 (2018).
- Kaczynska, K. & Szereda-Przestaszewska, M. The potential role of the nodose ganglion adenosine A₁ receptor in regulation of breathing in anaesthetized rats. *J. Physiol. Pharm.* **59**, 759–770 (2008).
- Koepfen, M., Eckle, T. & Eltzschig, H. K. Selective deletion of the A₁ adenosine receptor abolishes heart-rate slowing effects of intravascular adenosine in vivo. *PLoS ONE* **4**, e6784 (2009).
- Varani, K., Vincenzi, F., Merighi, S., Gessi, S. & Borea, P. A. Biochemical and pharmacological role of A₁ adenosine receptors and their modulation as novel therapeutic strategy. *Adv. Exp. Med. Biol.* **1051**, 193–232 (2017).
- Baltos, J. A. et al. Quantification of adenosine A₁ receptor biased agonism: Implications for drug discovery. *Biochem. Pharm.* **99**, 101–112 (2016).
- Weltha, L., Reemmer, J., Boison, D. The role of adenosine in epilepsy. *Brain Res. Bull.* **151**, 46–54 (2018).
- Deb, P. K., Deka, S., Borah, P., Abed, S. N. & Klotz, K. N. Medicinal chemistry and therapeutic potential of agonists, antagonists and allosteric modulators of A₁ adenosine receptor: current status and perspectives. *Curr. Pharm. Des.* **25**, 2697–2715 (2019).
- Kenakin, T. Biased receptor signaling in drug discovery. *Pharm. Rev.* **71**, 267–315 (2019).
- Wootten, D., Christopoulos, A., Marti-Solano, M., Babu, M. M. & Sexton, P. M. Mechanisms of signalling and biased agonism in G protein-coupled receptors. *Nat. Rev. Mol. Cell Biol.* **19**, 638–653 (2018).
- Violin, J. D. & Lefkowitz, R. J. Beta-arrestin-biased ligands at seven-transmembrane receptors. *Trends Pharm. Sci.* **28**, 416–422 (2007).
- Smith, J. S., Lefkowitz, R. J. & Rajagopal, S. Biased signalling: from simple switches to allosteric microprocessors. *Nat. Rev. Drug Discov.* **17**, 243–260 (2018).
- Foster, D. J. & Conn, P. J. Allosteric modulation of GPCRs: new insights and potential utility for treatment of schizophrenia and other CNS disorders. *Neuron* **94**, 431–446 (2017).
- Wingler, L. M. et al. Angiotensin and biased analogs induce structurally distinct active conformations within a GPCR. *Science* **367**, 888–892 (2020).
- Slosky, L. M., et al. Beta-arrestin-biased allosteric modulator of NTSR1 selectively attenuates addictive behaviors. *Cell* **181**, 1364–1379.e14 (2020).
- Kliwer, A. et al. Morphine-induced respiratory depression is independent of beta-arrestin2 signalling. *Br. J. Pharm.* **177**, 2923–2931 (2020).
- Yano, H. et al. Gs- versus Golf-dependent functional selectivity mediated by the dopamine D1 receptor. *Nat. Commun.* **9**, 486 (2018).
- Von Moo, E. et al. Ligand-directed bias of G protein signaling at the dopamine D2 receptor. *Cell Chem. Biol.* **29**, 226–238.e224 (2022).
- Luttrell, L. M., Maudsley, S. & Gesty-Palmer, D. Translating in vitro ligand bias into in vivo efficacy. *Cell Signal.* **41**, 46–55 (2018).
- Benredjem, B. et al. Exploring use of unsupervised clustering to associate signaling profiles of GPCR ligands to clinical response. *Nat. Commun.* **10**, 4075 (2019).
- Cordeaux, Y., Ijzerman, A. P. & Hill, S. J. Coupling of the human A₁ adenosine receptor to different heterotrimeric G proteins: evidence for agonist-specific G protein activation. *Br. J. Pharm.* **143**, 705–714 (2004).

30. Stewart, G. D. et al. Determination of adenosine A₁ receptor agonist and antagonist pharmacology using *Saccharomyces cerevisiae*: implications for ligand screening and functional selectivity. *J. Pharm. Exp. Ther.* **331**, 277–286 (2009).
31. Valant, C. et al. Separation of on-target efficacy from adverse effects through rational design of a bitopic adenosine receptor agonist. *Proc. Natl Acad. Sci. USA* **111**, 4614–4619 (2014).
32. Aurelio, L. et al. A Structure-Activity Relationship Study of Bitopic N(6)-Substituted Adenosine Derivatives as Biased Adenosine A₁ Receptor Agonists. *J. Med. Chem.* **61**, 2087–2103 (2018).
33. Knight, A. et al. Discovery of novel adenosine receptor agonists that exhibit subtype selectivity. *J. Med. Chem.* **59**, 947–964 (2016).
34. Jagtap P. Adenosine compounds and their use thereof Patent WO2011/119919 A1 (2011).
35. Jacobson, K. A. et al. A₃-adenosine receptors: design of selective ligands and therapeutic prospects. *Drugs Future* **20**, 689–699 (1995).
36. Angers, S. et al. Detection of β_2 -adrenergic receptor dimerization in living cells using bioluminescence resonance energy transfer (BRET). *Proc. Natl Acad. Sci.* **97**, 3684–3689 (2000).
37. Hamdan F. F., Percherancier Y., Breton B., Bouvier M. Monitoring protein-protein interactions in living cells by bioluminescence resonance energy transfer (BRET). *Curr Protoc Neurosci* **Chapter 5**, Unit 5.23 (2006).
38. Kocan, M. & Pflieger, K. D. Study of GPCR-protein interactions by BRET. *Methods Mol. Biol.* **746**, 357–371 (2011).
39. Pflieger, K. D., Seeber, R. M. & Eidne, K. A. Bioluminescence resonance energy transfer (BRET) for the real-time detection of protein-protein interactions. *Nat. Protoc.* **1**, 337–345 (2006).
40. Salahpour, A. et al. BRET biosensors to study GPCR biology, pharmacology, and signal transduction. *Front Endocrinol. (Lausanne)* **3**, 105 (2012).
41. Ciruela, F. et al. Ligand-induced phosphorylation, clustering, and desensitization of A₁ adenosine receptors. *Mol. Pharm.* **52**, 788–797 (1997).
42. Escriche, M. et al. Ligand-induced caveolae-mediated internalization of A₁ adenosine receptors: morphological evidence of endosomal sorting and receptor recycling. *Exp. Cell Res.* **285**, 72–90 (2003).
43. Ferguson, G., Watterson, K. R. & Palmer, T. M. Subtype-specific regulation of receptor internalization and recycling by the carboxyl-terminal domains of the human A₁ and rat A₃ adenosine receptors: consequences for agonist-stimulated translocation of arrestin3. *Biochemistry* **41**, 14748–14761 (2002).
44. Gines, S. et al. Involvement of caveolin in ligand-induced recruitment and internalization of A₁ adenosine receptor and adenosine deaminase in an epithelial cell line. *Mol. Pharm.* **59**, 1314–1323 (2001).
45. Iacovelli, L., Franchetti, R., Grisolia, D. & De Blasi, A. Selective regulation of G protein-coupled receptor-mediated signaling by G protein-coupled receptor kinase 2 in FRTL-5 cells: analysis of thyrotropin, α_{1B} -adrenergic, and A₁ adenosine receptor-mediated responses. *Mol. Pharm.* **56**, 316–324 (1999).
46. Yin, W. et al. A complex structure of arrestin-2 bound to a G protein-coupled receptor. *Cell Res.* **29**, 971–983 (2019).
47. Evans B. Adenosine Derivatives Patent EP0322242 (1989).
48. Gurden, M. F. et al. Functional characterization of three adenosine receptor types. *Br. J. Pharm.* **109**, 693–698 (1993).
49. Strong, P. et al. Suppression of non-esterified fatty acids and triacylglycerol in experimental animals by the adenosine analogue GR79236. *Clin. Sci. (Lond.)* **84**, 663–669 (1993).
50. Wise, A., Sheehan, M., Rees, S., Lee, M. & Milligan, G. Comparative analysis of the efficacy of A₁ adenosine receptor activation of Gi/o α G proteins following coexpression of receptor and G protein and expression of A₁ adenosine receptor-Gi/o α fusion proteins. *Biochemistry* **38**, 2272–2278 (1999).
51. Avet C., et al. Selectivity landscape of 100 therapeutically relevant GPCR profiled by an effector translocation-based BRET platform. *bioRxiv*, <https://www.biorxiv.org/content/10.1101/2020.04.20.052027v1> (2020).
52. Black, J. W. & Leff, P. Operational models of pharmacological agonism. *Proc. R. Soc. Lond. B Biol. Sci.* **220**, 141–162 (1983).
53. Gomes, I. et al. Biased signaling by endogenous opioid peptides. *Proc. Natl Acad. Sci. USA* **117**, 11820–11828 (2020).
54. Kenakin, T., Watson, C., Muniz-Medina, V., Christopoulos, A. & Novick, S. A simple method for quantifying functional selectivity and agonist bias. *ACS Chem. Neurosci.* **3**, 193–203 (2012).
55. Olsen, R. H. J. et al. TRUPATH, an open-source biosensor platform for interrogating the GPCR transducerome. *Nat. Chem. Biol.* **16**, 841–849 (2020).
56. Galés, C. et al. Probing the activation-promoted structural rearrangements in preassembled receptor-G protein complexes. *Nat. Struct. Mol. Biol.* **13**, 778–786 (2006).
57. Busnelli, M. et al. Functional selective oxytocin-derived agonists discriminate between individual G protein family subtypes. *J. Biol. Chem.* **287**, 3617–3629 (2012).
58. Tallarida R. J., Murray R. B. Analysis of the Regression Line. In: *Manual of Pharmacologic Calculations: With Computer Programs*. Springer New York (1987).
59. Kolasa, K., Harrell, L. E. & Parsons, D. S. Effects of pertussis toxin and galphaprotein-specific antibodies on phosphoinositide hydrolysis in rat brain membranes after cholinergic denervation and hippocampal sympathetic ingrowth. *Exp. Neurol.* **161**, 724–732 (2000).
60. Gilchrist, A., Li, A. & Hamm, H. E. G α COOH-terminal minigene vectors dissect heterotrimeric G protein signaling. *Sci. STKE* **2002**, pl1 (2002).
61. Gilchrist A., et al. Antagonists of the receptor-G protein interface block Gi-coupled signal transduction. *J. Biol. Chem.* **273**, 14912–14919 (1998).
62. McPherson, K. B. et al. Regulators of G-protein signaling (RGS) proteins promote receptor coupling to G-protein-coupled inwardly rectifying potassium (GIRK) channels. *J. Neurosci.* **38**, 8737–8744 (2018).
63. Ding, J. et al. RGS4-dependent attenuation of M4 autoreceptor function in striatal cholinergic interneurons following dopamine depletion. *Nat. Neurosci.* **9**, 832–842 (2006).
64. Vanhauwe, J. F. et al. Thrombin receptors activate Go proteins in endothelial cells to regulate intracellular calcium and cell shape changes. *J. Biol. Chem.* **277**, 34143–34149 (2002).
65. Goldsmith P., et al. Antibodies directed against synthetic peptides distinguish between GTP-binding proteins in neutrophil and brain. *J. Biol. Chem.* **262**, 14683–14688 (1987).
66. Mousli, M., Bronner, C., Bockaert, J., Rouot, B. & Landry, Y. Interaction of substance P, compound 48/80 and mastoparan with the alpha-subunit C-terminus of G protein. *Immunol. Lett.* **25**, 355–357 (1990).
67. McIntire, W. E., Dingus, J., Schey, K. L. & Hildebrandt, J. D. Characterization of the major bovine brain Go α isoforms. Mapping the structural differences between the alpha subunit isoforms identifies a variable region of the protein involved in receptor interactions. *J. Biol. Chem.* **273**, 33135–33141 (1998).
68. Oleskevich, S. G α o1 decapeptide modulates the hippocampal 5-HT1A potassium current. *J. Neurophysiol.* **74**, 2189–2193 (1995).
69. Rouot, B. et al. Specific antibodies against Go isoforms reveal the early expression of the Go2 α subunit and appearance of Go1 α during neuronal differentiation. *Mol. Pharm.* **41**, 273–280 (1992).
70. Oleskevich, S., Leck, K. J., Matthaai, K. & Hendry, I. A. Enhanced serotonin response in the hippocampus of Galphaz protein knock-out mice. *Neuroreport* **16**, 921–925 (2005).
71. Deganutti, G. et al. Deciphering the agonist binding mechanism to the adenosine A₁ Receptor. *ACS Pharm. Transl. Sci.* **4**, 314–326 (2021).
72. Cheng, R. K. Y. et al. Structures of human A₁ and A_{2A} adenosine receptors with xanthines reveal determinants of selectivity. *Structure* **25**, 1275–1285.e1274 (2017).
73. Bussi, G. & Laio, A. Using metadynamics to explore complex free-energy landscapes. *Nat. Rev. Phys.* **2**, 200–212 (2020).
74. Flock, T. et al. Selectivity determinants of GPCR-G-protein binding. *Nature* **545**, 317–322 (2017).
75. Okashah, N. et al. Variable G protein determinants of GPCR coupling selectivity. *Proc. Natl Acad. Sci. USA* **116**, 12054–12059 (2019).
76. Dror, R. O. et al. Activation mechanism of the β_2 -adrenergic receptor. *Proc. Natl. Acad. Sci. USA* **108**, 18684–18689 (2011).
77. Draper-Joyce, C. J. et al. Structure of the adenosine-bound human adenosine A₁ receptor-Gi complex. *Nature* **558**, 559–563 (2018).
78. Glukhova, A. et al. Structure of the adenosine A₁ receptor reveals the basis for subtype selectivity. *Cell* **168**, 867–877 e813 (2017).
79. Rosenbaum, D. M., Rasmussen, S. G. & Kobilka, B. K. The structure and function of G-protein-coupled receptors. *Nature* **459**, 356–363 (2009).
80. Kato, H. E. et al. Conformational transitions of a neurotensin receptor 1-Gi1 complex. *Nature* **572**, 80–85 (2019).
81. Liu, X. et al. Structural insights into the process of GPCR-G protein complex formation. *Cell* **177**, 1243–1251 e1212 (2019).
82. Kooistra, A. J. et al. GPCRdb in 2021: integrating GPCR sequence, structure and function. *Nucleic Acids Res.* **49**, D335–D343 (2020).
83. GPCRdb. Human A₁R mutations. https://gpcrdb.org/mutations/protein/aa1r_human/ (2020).
84. Asano, T. et al. The G-protein Go in mammalian cardiac muscle: localization and coupling to A₁ adenosine receptors. *J. Biochem* **117**, 183–189 (1995).
85. Wolf, W. P., Spicher, K., Haase, H. & Schulze, W. Immunocytochemical localization of the G-protein sub-unit, Go α , in rat heart. Implications for a role of Go α in secretion of cardiac hormones. *J. Mol. Cell Cardiol.* **30**, 1149–1162 (1998).
86. McGrath, M. F. & de Bold, A. J. Transcriptional analysis of the mammalian heart with special reference to its endocrine function. *BMC Genomics* **10**, 254 (2009).
87. Jiang, M. & Bajpayee, N. S. Molecular mechanisms of Go signaling. *Neurosignals* **17**, 23–41 (2009).

88. Kawai, Y. & Arinze, I. J. Differential localization and development-dependent expression of G-protein subunits, Go alpha and G beta, in rabbit heart. *J. Mol. Cell Cardiol.* **28**, 1555–1564 (1996).
89. Belardinelli, L., Shryock, J. C., Song, Y., Wang, D. & Srinivas, M. Ionic basis of the electrophysiological actions of adenosine on cardiomyocytes. *FASEB J.* **9**, 359–365 (1995).
90. Kim, S. H. & Chung, J. M. An experimental model for peripheral neuropathy produced by segmental spinal nerve ligation in the rat. *Pain* **50**, 355–363 (1992).
91. Fayaz, A., Croft, P., Langford, R. M., Donaldson, L. J. & Jones, G. T. Prevalence of chronic pain in the UK: a systematic review and meta-analysis of population studies. *BMJ Open* **6**, e010364 (2016).
92. Yong R. J., Mullins P. M., Bhattacharyya N. Prevalence of chronic pain among adults in the United States. *Pain* **163**, e328–e332 (2021).
93. Vos, T. et al. Global, regional, and national incidence, prevalence, and years lived with disability for 328 diseases and injuries for 195 countries, 1990–2016: a systematic analysis for the Global Burden of Disease Study 2016. *Lancet* **390**, 1211–1259 (2017).
94. Chincholkar, M. Analgesic mechanisms of gabapentinoids and effects in experimental pain models: a narrative review. *Br. J. Anaesth.* **120**, 1315–1334 (2018).
95. Li, A. H., Moro, S., Melman, N., Ji, X. D. & Jacobson, K. A. Structure-activity relationships and molecular modeling of 3, 5-diacyl-2,4-dialkylpyridine derivatives as selective A₃ adenosine receptor antagonists. *J. Med. Chem.* **41**, 3186–3201 (1998).
96. Alnouri, M. W. et al. Selectivity is species-dependent: characterization of standard agonists and antagonists at human, rat, and mouse adenosine receptors. *Purinergic Signal* **11**, 389–407 (2015).
97. Chen, Z. et al. Controlling murine and rat chronic pain through A₃ adenosine receptor activation. *FASEB J.* **26**, 1855–1865 (2012).
98. Ford, A. et al. Engagement of the GABA to KCC2 signaling pathway contributes to the analgesic effects of A₃AR agonists in neuropathic pain. *J. Neurosci.* **35**, 6057–6067 (2015).
99. Lucarini, E. et al. Acute visceral pain relief mediated by A₃AR agonists in rats: involvement of N-type voltage-gated calcium channels. *Pain* **161**, 2179–2190 (2020).
100. Imlach, W. L., Bhola, R. F., May, L. T., Christopoulos, A. & Christie, M. J. A positive allosteric modulator of the adenosine A₁ receptor selectively inhibits primary afferent synaptic transmission in a neuropathic pain model. *Mol. Pharm.* **88**, 460–468 (2015).
101. Little, J. W. et al. Endogenous adenosine A₃ receptor activation selectively alleviates persistent pain states. *Brain* **138**, 28–35 (2015).
102. Dunwiddie, T. V., Diao, L., Kim, H. O., Jiang, J. L. & Jacobson, K. A. Activation of hippocampal adenosine A₃ receptors produces a desensitization of A₁ receptor-mediated responses in rat hippocampus. *J. Neurosci.* **17**, 607–614 (1997).
103. Colca, J. R. Discontinued drugs 2011: endocrine and metabolic. *Expert Opin. Investig. Drugs* **21**, 1619–1624 (2012).
104. Fathollahi, M. et al. A novel partial agonist of the A₁ adenosine receptor and evidence of receptor homogeneity in adipocytes. *J. Pharmacol. Exp. Ther.* **317**, 676–684 (2006).
105. Drury, A. N. & Szent-Gyorgyi, A. The physiological activity of adenine compounds with especial reference to their action upon the mammalian heart. *J. Physiol.* **68**, 213–237 (1929).
106. Finnerup, N. B. et al. Neuropathic pain clinical trials: factors associated with decreases in estimated drug efficacy. *Pain* **159**, 2339–2346 (2018).
107. Imam, M. Z., Kuo, A., Ghassabian, S. & Smith, M. T. Progress in understanding mechanisms of opioid-induced gastrointestinal adverse effects and respiratory depression. *Neuropharmacology* **131**, 238–255 (2018).
108. Wall, M. J. & Dale, N. Neuronal transporter and astrocytic ATP exocytosis underlie activity-dependent adenosine release in the hippocampus. *J. Physiol.* **591**, 3853–3871 (2013).
109. Anderson, W. W. & Collingridge, G. L. Capabilities of the WinLTP data acquisition program extending beyond basic LTP experimental functions. *J. Neurosci. Methods* **162**, 346–356 (2007).
110. Frenguelli, B. G. & Wall, M. J. Combined electrophysiological and biosensor approaches to study purinergic regulation of epileptiform activity in cortical tissue. *J. Neurosci. Methods* **260**, 202–214 (2016).
111. Weston, C. et al. Receptor activity-modifying protein-directed G protein signaling specificity for the calcitonin gene-related peptide family of receptors. *J. Biol. Chem.* **291**, 25763 (2016).
112. Barkan, K. et al. Pharmacological characterisation of novel adenosine receptor A₃R antagonists. *Sci. Rep.* **27**, 20781 (2019).
113. Stoddart, L. A. et al. Fragment screening at adenosine-A₃ receptors in living cells using a fluorescence-based binding assay. *Chem. Biol.* **19**, 1105–1115 (2012).
114. Vernall, A. J., Stoddart, L. A., Bridson, S. J., Hill, S. J. & Kellam, B. Highly potent and selective fluorescent antagonists of the human adenosine A₃ receptor based on the 1,2,4-triazolo[4,3-a]quinoxalin-1-one scaffold. *J. Med. Chem.* **55**, 1771–1782 (2012).
115. Stoddart, L. A. et al. Application of BRET to monitor ligand binding to GPCRs. *Nat. Methods* **12**, 661–663 (2015).
116. Huang, J. & MacKerell, A. D. CHARMM36 all-atom additive protein force field: validation based on comparison to NMR data. *J. Comput. Chem.* **34**, 2135–2145 (2013).
117. Huang, J. et al. CHARMM36m: an improved force field for folded and intrinsically disordered proteins. *Nat. Methods* **14**, 71–73 (2017).
118. Vanommeslaeghe, K. & MacKerell, A. D. Jr. Automation of the CHARMM General Force Field (CGenFF) I: bond perception and atom typing. *J. Chem. Inf. Model.* **52**, 3144–3154 (2012).
119. Vanommeslaeghe, K., Raman, E. P. & MacKerell, A. D. Automation of the CHARMM General Force Field (CGenFF) II: assignment of bonded parameters and partial atomic charges. *J. Chem. Inf. Model.* **52**, 3155–3168 (2012).
120. Yu, W., He, X., Vanommeslaeghe, K. & MacKerell, A. D. Extension of the CHARMM general force field to sulfonyl-containing compounds and its utility in biomolecular simulations. *J. Comput. Chem.* **33**, 2451–2468 (2012).
121. Doerr, S., Harvey, M. J., Noé, F. & De Fabritiis, G. HTMD: high-throughput molecular dynamics for molecular discovery. *J. Chem. Theory Comput.* **12**, 1845–1852 (2016).
122. Humphrey, W., Dalke, A. & Schulten, K. VMD: visual molecular dynamics. *J. Mol. Graph.* **14**, 33–38 (1996). 27–38.
123. Mayne, C. G., Saam, J., Schulten, K., Tajkhorshid, E. & Gumbart, J. C. Rapid parameterization of small molecules using the Force Field Toolkit. *J. Comput. Chem.* **34**, 2757–2770 (2013).
124. Berman, H., Henrick, K. & Nakamura, H. Announcing the worldwide Protein Data bank. *Nat. Struct. Biol.* **10**, 980 (2003).
125. Berman, H. M. et al. The protein data bank. *Nucleic Acids Res* **28**, 235–242 (2000).
126. Fiser, A. & Sali, A. Modeller: generation and refinement of homology-based protein structure models. *Methods Enzymol.* **374**, 461–491 (2003).
127. Sali, A. & Blundell, T. L. Comparative protein modelling by satisfaction of spatial restraints. *J. Mol. Biol.* **234**, 779–815 (1993).
128. Dal Maso, E. et al. Extracellular loops 2 and 3 of the calcitonin receptor selectively modify agonist binding and efficacy. *Biochem. Pharmacol.* **150**, 214–244 (2018).
129. Liang, Y.-L. et al. Cryo-EM structure of the active, Gs-protein complexed, human CGRP receptor. *Nature* **561**, 492–497 (2018).
130. Dolinsky, T. J., Nielsen, J. E., McCammon, J. A. & Baker, N. A. PDB2PQR: an automated pipeline for the setup of Poisson-Boltzmann electrostatics calculations. *Nucleic Acids Res.* **32**, W665–667 (2004).
131. Olsson, M. H. M., Søndergaard, C. R., Rostkowski, M. & Jensen, J. H. PROPKA3: consistent treatment of internal and surface residues in empirical pK predictions. *J. Chem. Theory Comput.* **7**, 525–537 (2011).
132. Sommer, B. Membrane packing problems: a short review on computational membrane modeling methods and tools. *Comput. Struct. Biotechnol. J.* **5**, e201302014 (2013).
133. Lomize, M. A., Lomize, A. L., Pogozheva, I. D. & Mosberg, H. I. OPM: orientations of proteins in membranes database. *Bioinformatics* **22**, 623–625 (2006).
134. Jorgensen, W. L., Chandrasekhar, J., Madura, J. D., Impey, R. W. & Klein, M. L. Comparison of simple potential functions for simulating liquid water. *J. Chem. Phys.* **79**, 926 (1983).
135. Harvey, M. J., Giupponi, G. & Fabritiis, G. D. ACEMD: accelerating biomolecular dynamics in the microsecond time scale. *J. Chem. Theory Comput.* **5**, 1632–1639 (2009).
136. Berendsen, H. J. C., Postma, J. P. M., van Gunsteren, W. F., DiNola, A. & Haak, J. R. Molecular dynamics with coupling to an external bath. *J. Chem. Phys.* **81**, 3684 (1984).
137. Loncharich, R. J., Brooks, B. R. & Pastor, R. W. Langevin dynamics of peptides: the frictional dependence of isomerization rates of N-acetylalanine-N-methylamide. *Biopolymers* **32**, 523–535 (1992).
138. Deganutti, G. & Moro, S. Estimation of kinetic and thermodynamic ligand-binding parameters using computational strategies. *Future Med. Chem.* **9**, 507–523 (2017).
139. Sabbadin D., Salmasso V., Sturlese M., Moro S. Supervised molecular dynamics (sumd) approaches in drug design 1824:287–298 (2018).
140. Cuzzolin, A. et al. Deciphering the complexity of ligand-protein recognition pathways using supervised molecular dynamics (SuMD) simulations. *J. Chem. Inf. Model.* **56**, 687–705 (2016).
141. Deganutti, G., Cuzzolin, A., Ciancetta, A. & Moro, S. Understanding allosteric interactions in G protein-coupled receptors using supervised molecular dynamics: a prototype study analysing the human A₃ adenosine receptor positive allosteric modulator LUF6000. *Bioorg. Med. Chem.* **23**, 4065–4071 (2015).

142. Deganutti, G. & Moro, S. Supporting the identification of novel fragment-based positive allosteric modulators using a supervised molecular dynamics approach: a retrospective analysis considering the human A_{2A} adenosine receptor as a key example. *Molecules* **22**, 818 (2017).
143. Deganutti G., Salmaso V., Moro S. Could adenosine recognize its receptors with a stoichiometry other than 1:1? *Mol Inform* **37**, e1800009 (2018).
144. Deganutti, G., Welihinda, A. & Moro, S. Comparison of the human A_{2A} adenosine receptor recognition by adenosine and inosine: new insight from supervised molecular dynamics simulations. *ChemMedChem* **12**, 1319–1326 (2017).
145. Sabbadin, D. & Moro, S. Supervised molecular dynamics (SuMD) as a helpful tool to depict GPCR-ligand recognition pathway in a nanosecond time scale. *J. Chem. Inf. Model* **54**, 372–376 (2014).
146. Salmaso, V., Sturlese, M., Cuzzolin, A. & Moro, S. Exploring protein-peptide recognition pathways using a supervised molecular dynamics approach. *Structure* **25**, 655–662.e652 (2017).
147. Branduardi, D., Gervasio, F. L. & Parrinello, M. From A to B in free energy space. *J. Chem. Phys.* **126**, 054103 (2007).
148. Laio, A. & Parrinello, M. Escaping free-energy minima. *Proc. Natl Acad. Sci. USA* **99**, 12562–12566 (2002).
149. Laio, A., Rodriguez-Fortea, A., Gervasio, F. L., Ceccarelli, M. & Parrinello, M. Assessing the accuracy of metadynamics. *J. Phys. Chem. B* **109**, 6714–6721 (2005).
150. Tribello, G. A., Bonomi, M., Branduardi, D., Camilloni, C. & Bussi, G. PLUMED 2: New feathers for an old bird. *Comput. Phys. Commun.* **185**, 604–613 (2014).
151. Deganutti, G. et al. Impact of protein–ligand solvation and desolvation on transition state thermodynamic properties of adenosine A_{2A} ligand binding kinetics. *Silico Pharm.* **5**, 16 (2016).
152. Barducci, A., Bussi, G. & Parrinello, M. Well-tempered metadynamics: a smoothly converging and tunable free-energy method. *Phys. Rev. Lett.* **100**, 020603 (2008).
153. Baker, J. G. & Hill, S. J. A comparison of the antagonist affinities for the Gi- and Gs-coupled states of the human adenosine A₁ receptor. *J. Pharm. Exp. Ther.* **320**, 218–228 (2007).
154. Hill, S. J. & Baker, J. G. The ups and downs of Gs- to Gi-protein switching. *Br. J. Pharm.* **138**, 1188–1189 (2003).
155. Klein Herenbrink, C. et al. The role of kinetic context in apparent biased agonism at GPCRs. *Nat. Commun.* **7**, 10842 (2016).

Acknowledgements

We gratefully acknowledge the support of the University of Warwick (URSS Awards to S.H. and J.O.; Warwick Ventures Proof of Concept Fund awards to M.J.W. & B.G.F.), the Leverhulme Trust (RPG-2017-255, CAR and G.L. to fund K.B. and G.D.), the BBSRC (BB/M00015X/2, G.L., and BB/M01116X/1, Ph.D. studentship to E.H.), the MRC (MR/J003964/1; I.W. and 2270402, iCASE PhD Studentship with NeuroSolutions to C.L.M.) and The Swiss National Science Foundation (PP00P2_123536 and PP00P2_146321, M.Lo). A.S. is supported by a European Scholarship from the Cambridge Trust, S.C. is funded by an AstraZeneca Ph.D. studentship and X.H. is funded by a China Scholarship Council Cambridge International Scholarship. R.H. is supported by an MRC Discovery Award (MC_PC_15070). C.A.R. is a Royal Society Industry Fellow. We would like to thank: Stephen Hill, Stephen Briddon, and Mark Soave (University of Nottingham) for gifting the Nluc-tagged adenosine receptor cell lines, the fluorescent antagonist AV039, and technical advice; Kathleen Caron and Duncan Mackie (University of North Carolina) for the β-arrestin1/2-YFP constructs, and Annette Gilchrist (Midwestern University) and Heidi Hamm (Vanderbilt University) for assistance with the Gao interfering

peptide plasmids. We are grateful to Kevin Moffat and the Biochemistry students of the School of Life Sciences at the University of Warwick for access to their frog heart preparations; Nick Dale, Mark Wigglesworth, Jens Kleinjung for discussions and comments on draft manuscripts, and Arthur Christopoulos for a pre-publication copy of the adenosine A_{1R} cryo-EM structure. In vivo studies on neuropathic pain were funded and undertaken by NeuroSolutions Ltd. Illustrative figures in Figs. 1b, c; 2a–d, i, j; 3i, j; 5a; 6a; 7a, b were created with BioRender.com. Venn diagram in Fig. 2e was made at <http://bioinformatics.psb.ugent.be/webtools/Venn/>.

Author contributions

Experiments were designed by M.J.W., R.H., G.D., C.A.R., G.L., F.Y.Z., W.I., D.Sp., B.G.F., and were performed by M.J.W., E.H., R.H., K.B., I.W., S.C., A.S., H.F.W., D.Sa., X.H., W.I., C.L.M., E.D., C.H., S.H., J.O. Compounds were synthesised by M.L.E., B.P., M.Lo. Molecular dynamics and docking simulations were designed and carried out by G.D. and C.A.R. Work was originally conceived by M.J.W. and B.G.F. The manuscript was written by M.J.W., G.D., C.A.R., G.L., B.G.F., with valuable input from E.H., R.H., K.B., M.Lo., I.W., W.I. and D.Sp.

Competing interests

The University of Warwick has filed a patent application for uses of BnOCPA in which M.W. and B.G.F. are named as the inventors and M.Lo., R.H., G.L., D.Sp., C.A.R. and G.D. are named as contributors. F.Y.Z., H.F.W., and D.Sp. are employees and/or hold shares in NeuroSolutions, which holds a licence to this patent. The remaining authors declare no competing interests.

Additional information

Supplementary information The online version contains supplementary material available at <https://doi.org/10.1038/s41467-022-31652-2>.

Correspondence and requests for materials should be addressed to Mark J. Wall, Graham Ladds or Bruno G. Frenguelli.

Peer review information *Nature Communications* thanks Kenneth Jacobson, Daniela Salvemini and the anonymous reviewer(s) for their contribution to the peer review of this work.

Reprints and permission information is available at <http://www.nature.com/reprints>

Publisher's note Springer Nature remains neutral with regard to jurisdictional claims in published maps and institutional affiliations.



Open Access This article is licensed under a Creative Commons Attribution 4.0 International License, which permits use, sharing, adaptation, distribution and reproduction in any medium or format, as long as you give appropriate credit to the original author(s) and the source, provide a link to the Creative Commons license, and indicate if changes were made. The images or other third party material in this article are included in the article's Creative Commons license, unless indicated otherwise in a credit line to the material. If material is not included in the article's Creative Commons license and your intended use is not permitted by statutory regulation or exceeds the permitted use, you will need to obtain permission directly from the copyright holder. To view a copy of this license, visit <http://creativecommons.org/licenses/by/4.0/>.

© The Author(s) 2022